Article

Cell Reports

RAB-5- and DYNAMIN-1-Mediated Endocytosis of EFF-1 Fusogen Controls Cell-Cell Fusion

Graphical Abstract

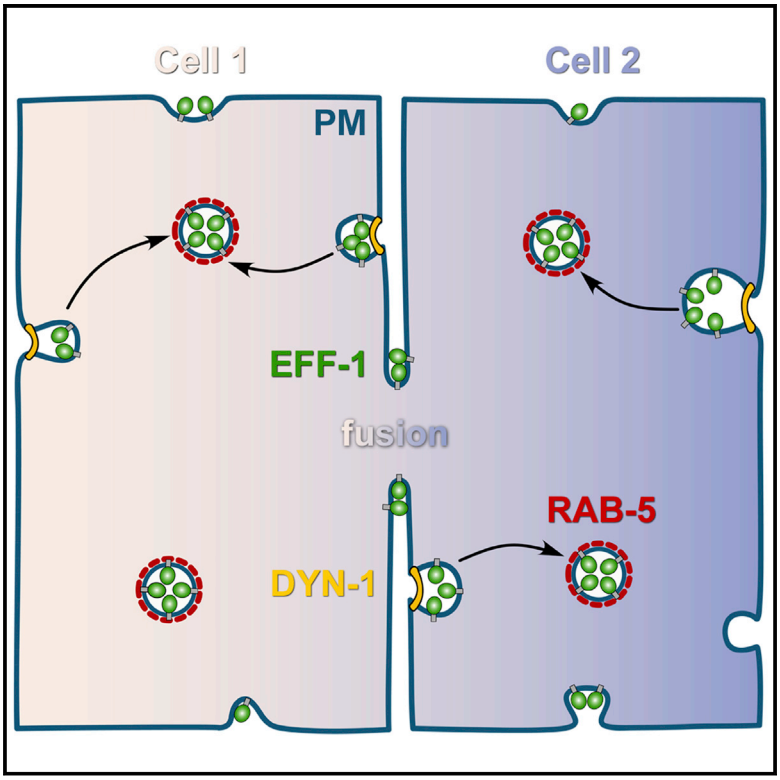

Authors

Ksenia Smurova, Benjamin Podbilewicz

Correspondence

podbilew@technion.ac.il

In Brief

Smurova and Podbilewicz find that RAB-5 and dynamin-mediated endocytosis removes the fusogen EFF-1 from the plasma membrane and serves as a negative regulator of cell-cell fusion in *C. elegans* embryos. Thus, dynamic and transient localization of EFF-1 on the apical plasma membranes is sufficient to merge neighboring cells.

Highlights

- The fusion protein EFF-1 is targeted to early endosomes
- Dynamin and RAB-5 downregulate EFF-1 in *C. elegans* embryos
- Transient and dynamic localization of EFF-1 to apical cell membranes mediates fusion
- Prevention of EFF-1 endocytosis induces excessive cell fusion

Smurova & Podbilewicz, 2016, Cell Reports *14*, 1517–1527
February 16, 2016
http://dx.doi.org/10.1016/j.celrep.2016.01.027

CellPress

Cell Reports
Article

RAB-5- and DYNAMIN-1-Mediated Endocytosis of EFF-1 Fusogen Controls Cell-Cell Fusion

Ksenia Smurova[1] and Benjamin Podbilewicz[1,*]
[1]Department of Biology, Technion-Israel Institute of Technology, Haifa 32000, Israel
*Correspondence: podbilew@technion.ac.il
http://dx.doi.org/10.1016/j.celrep.2016.01.027

SUMMARY

Cell-cell fusion plays essential roles during fertilization and organogenesis. Previous studies in *C. elegans* led to the identification of the eukaryotic fusion protein (EFF-1 fusogen), which has structural homology to class II viral fusogens. Transcriptional repression of EFF-1 ensures correct fusion fates, and overexpression of EFF-1 results in embryonic lethality. EFF-1 must be expressed on the surface of both fusing cells; however, little is known regarding how cells regulate EFF-1 surface exposure. Here, we report that EFF-1 is actively removed from the plasma membrane of epidermal cells by dynamin- and RAB-5-dependent endocytosis and accumulates in early endosomes. EFF-1 was transiently localized to apical domains of fusion-competent cells. Effective cell-cell fusion occurred only between pairs of cell membranes in which EFF-1 localized. Downregulation of dynamin or RAB-5 caused EFF-1 mislocalization to all apical membrane domains and excessive fusion. Thus, internalization of EFF-1 is a safety mechanism preventing excessive cell fusion.

INTRODUCTION

Cell-to-cell fusion initiates the process of sexual reproduction and, following fertilization, sculpts organs such as muscle, bone, eye lens, and placenta in the developing organism (Aguilar et al., 2013). Cell fusion is also involved in inflammation, regeneration, wound healing, and cancer (Losick et al., 2013; Medvinsky and Smith, 2003; Oren-Suissa and Podbilewicz, 2010; Rizvi et al., 2006). Nevertheless, little is known about mechanisms that regulate cell fusion (Chen et al., 2007; Podbilewicz, 2014). In the nematode *Caenorhabditis elegans*, one-third of all somatic cells fuse during development, making this organism attractive for studying cell fusion (Gattegno et al., 2007; Podbilewicz and White, 1994; Shinn-Thomas and Mohler, 2011). The first identified eukaryotic fusogen, the *C. elegans* epithelial fusion failure 1 (EFF-1), mediates fusion of cells in the hypodermis (skin), pharynx, and vulva (Mohler et al., 2002). Ectopic expression of EFF-1 can induce fusion of cells that normally do not fuse both in *C. elegans* and in heterologous cells grown in culture (Avinoam et al., 2011; Podbilewicz et al., 2006; Shemer et al., 2004). Fusion of these cells requires EFF-1 expression in both fusing partners (Avinoam et al., 2011; Kim et al., 2015; Podbilewicz et al., 2006; Shilagardi et al., 2013). Because EFF-1 is a potent fusogen and its ectopic expression induces embryonic lethality, it must be regulated in space and time. Different genetic pathways including Engrailed/CEH-16, GATA factors, Hox, Notch, RTK, and Wnt signaling regulate *eff*-1 activity directly or indirectly (Alper and Kenyon, 2002; Brabin et al., 2011; Cassata et al., 2005; Fernandes and Sternberg, 2007; Kontani et al., 2005; Margalit et al., 2007; Pellegrino et al., 2011; Rasmussen et al., 2008; Shemer and Podbilewicz, 2002; Walser et al., 2006; Weinstein and Mendoza, 2013). However, very little is known about EFF-1 regulation at the protein level.

We aimed to understand which cellular mechanisms are involved in EFF-1 posttranslational regulation. The endocytic pathway controls numerous cellular processes including signaling pathways, epithelial polarity, cellular remodeling, synaptic transmission, cancer, and osteoclast and myoblast fusion (Chen et al., 2006; Fares and Greenwald, 2001; Grant and Hirsh, 1999; Leikina et al., 2013; Luga et al., 2012; Mellman and Yarden, 2013; Sato and Sato, 2013; Shin et al., 2014; Watanabe et al., 2013). Researchers have uncovered the role of actin, lipids, membrane curvature-modulating proteins, and dynamin in clathrin-dependent and -independent pathways of endocytosis (Kozlov et al., 2014; McMahon and Boucrot, 2011; Messa et al., 2014; Schmid et al., 2014). Rab proteins, small GTP-binding proteins of the Ras superfamily, control trafficking between organelles, including the ER, Golgi, plasma membrane, endosomes, and lysosomes (Grant and Donaldson, 2009; Mellman, 1996; Mizuno-Yamasaki et al., 2012). The Rab5 GTPase was shown to be a central regulator of the endolysosomal system as loss of Rab5 function caused a reduction in the number of endosomes and lysosomes and associated block of endocytosis (Zeigerer et al., 2012). However, little is known about membrane trafficking during developmental cell fusion.

Here, we show that endocytosis regulates homotypic EFF-1-mediated cell-cell fusion in *C. elegans* embryos. EFF-1 colocalizes with RAB-5 in early endosomes before and during fusion, whereas RAB-5 depletion results in EFF-1 mislocalization to the apical plasma membrane and induces ectopic fusion. EFF-1 localization at the apical plasma membrane is dynamic and transient due to its downregulation by dynamin- and RAB-5-dependent endocytosis. Membrane merger is initiated only

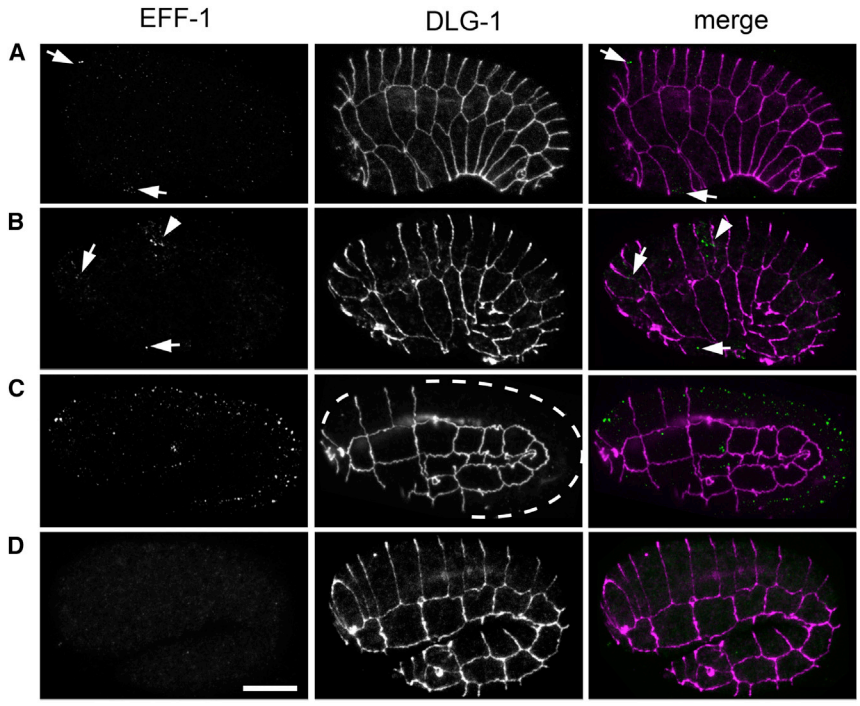

Figure 1. EFF-1 Localizes to Intracellular Puncta

(A–C) EFF-1 expression pattern in the process of cell fusion was revealed by immunostaining with anti-EFF-1 monoclonal antibody (green) and anti-DLG-1 antibody (apical junctions, magenta). EFF-1 vesicular localization (arrows) at developmental stages prior to (A and B) and after epithelial cell fusion (C) in wild-type *C. elegans* embryos is shown. Colocalization of EFF-1 with apical junction is shown (arrowhead; B). Fused *hyp6* and *hyp7* syncytia are outlined with a white dashed line in (C).

(D) Immunostaining of *eff-1*(*ok1021*) mutant at 1.8-fold stage shows no EFF-1 expression, revealing the antibody specificity, and lack of cell fusion. The scale bar represents 10 μm.

(E) Schematics of embryonic epithelial cell fusions during elongation from comma (left) to 1.8-fold stage (right). Cell borders (junctions) are drawn with black lines; EFF-1 expression pattern is visualized as green puncta. Cells forming *hyp6* and *hyp7* syncytia are colored with dark gray and light gray, respectively.

Orientation of embryos in all figures is anterior, left and dorsal, top. See also Figure S1.

when both apposing apical plasma membranes co-express EFF-1.

RESULTS

EFF-1 Localizes to Intracellular Puncta

To uncover the expression pattern of the EFF-1 protein during development, its endogenous localization was followed by immunofluorescence with specific monoclonal antibodies against the extracellular domain of EFF-1 (Fridman, 2012; K. Fridman, C. Valansi, O. Avinoam, M. Oren, D. Pérez, C. Sánchez Espinel, Á. González-Fernández, A. Rotem, A. Harel, T. Krey, F.A. Rey, J.M. White, and B.P., unpublished data). EFF-1 was first detected at the bean stage within individual puncta in the dorsal and ventral hypodermal cells before fusion (n = 14; Figure 1A, arrows). Subsequently, EFF-1 appeared as punctate staining in the cytoplasm of hyp6 and hyp7 precursor cells at the comma stage (n = 18; Figure 1B, arrows). Following embryonic fusions, EFF-1 remained vesicular, and the number of EFF-1 puncta increased when cell fusion was nearly completed (n = 20; Figure 1C). EFF-1 puncta showed minor co-localization with apical cell junctions detected by anti-DLG-1 antibody (Figure 1B, arrowhead). We found that EFF-1 puncta were aligned along longitudinal lines lying parallel to the seam cells (Figure 1C). This arrangement might be dictated by the organization of the cytoskeleton in the syncytial hypodermal cells, where actin, intermediate filaments, and microtubules form bundles that run parallel to the seam cells (Figure S1). *eff-1*(*ok1021*)-null embryos at any stages did not show immunoreactivity, revealing the specificity of the monoclonal antibodies (Figure 1D). Thus, EFF-1 is expressed in puncta at the onset, during, and after hypodermal cell fusion in developing embryos (Figure 1E).

RAB-5 and DYN-1 RNAi Induce EFF-1 Plasma Membrane Accumulation

To follow the dynamics of EFF-1 expression in live embryos, we generated a transgenic strain carrying a fosmid-based reporter construct containing the entire EFF-1 locus fused to GFP, as well as ~10 kb of upstream and downstream *cis*-regulatory regions (Sarov et al., 2012). The EFF-1::GFP fosmid was injected into the *eff-1*(*hy21ts*) mutant to prevent lethality induced by overexpression of EFF-1. Because EFF-1::GFP rescued the fusion failure mutant phenotype, we assumed that EFF-1::GFP was active and its expression level was similar to the endogenous EFF-1 level. Most of the EFF-1 protein localizes to intracellular puncta both before and during the fusion process (Figure 2A; Movies S1 and S2). To understand whether EFF-1 vesicular localization at steady state is dependent on rapid internalization from the plasma membrane, we hypothesized that reducing endocytic efficiency will result in localization of EFF-1 to the plasma membrane. We depleted *rab-5*, an essential regulator of endocytosis, using RNAi and followed EFF-1::GFP by live imaging. We found that *rab-5* RNAi embryos showed enrichment of EFF-1::GFP in apical plasma membrane domain, rather than the bright organelles observed in the control embryos (Figures 2A–2D; Movies S3 and S4). In control embryos, there was only

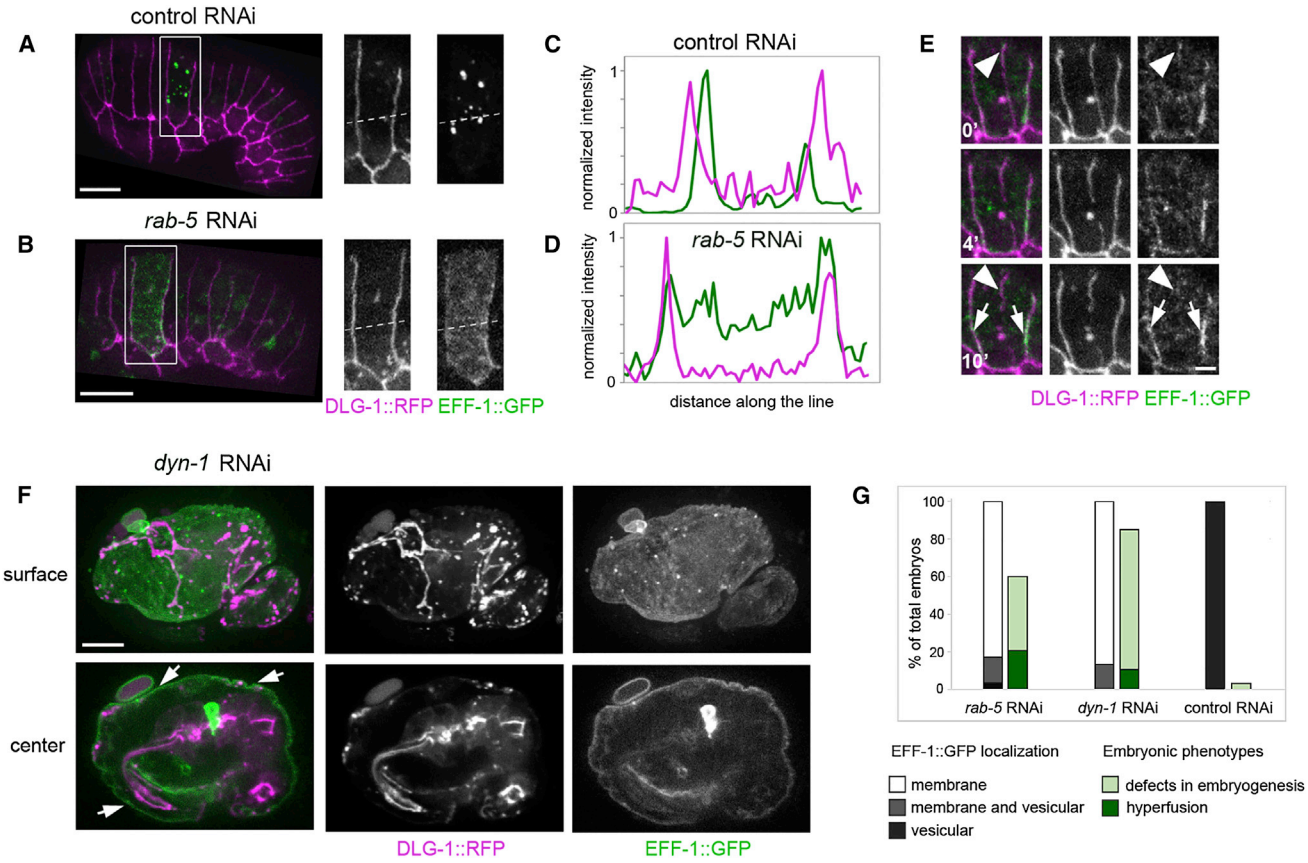

Figure 2. RAB-5 and DYN-1 RNAi Knockdown Induces EFF-1 Accumulation on the Apical Plasma Membrane

(A, B, and F) Live images of EFF-1::GFP (green) and apical junctions, DLG-1::RFP (magenta) in embryos treated with control RNAi (A), *rab-5* RNAi (B), and *dyn-1* RNAi (F). Right panel represents the magnified region of the inset area in (A) and (B).

(A) EFF-1::GFP is in puncta in control RNAi. See also Movies S1 and S2.

(B) EFF-1::GFP in *rab-5* RNAi embryo appears diffuse on the cytoplasm in smaller vesicles and associated with the apical plasma membranes and junctions. See also Figure S2G and Movies S3 and S4.

(C) Intensity profile plotted along the line (white dashed line in A) of EFF-1::GFP (green line on the plot) and DLG-1::RFP (magenta line on the plot) shows no correlation.

(D) Intensity profiles plotted along dashed line from (B) represent correlation of EFF-1::GFP and DLG-1::RFP intensities on the cell junctions, showing the enrichment of EFF-1::GFP on the apical plasma membrane.

(E) Representative stages from time-lapse images of cell fusion under *rab-5* RNAi showing EFF-1::GFP/DLG-1::RFP colocalization (arrows). Cell junction undergoing fusion is marked by an arrowhead. Note that EFF-1 dissociated from the cell junction at 10 min of fusion (arrowhead). Time in min is indicated. See also Movie S3.

(F) EFF-1::GFP apical plasma membrane expression (arrows) caused by *dyn-1* RNAi is shown on the embryo surface focus (upper panels) and center focus (lower panels). Embryogenesis defects and hyperfusion are visualized by DLG-1::RFP pattern (Movie S5).

(G) EFF-1 localization and embryonic defects caused by *rab-5* and *dyn-1* downregulation. The first bar graph represents percentage of embryos showing EFF-1 localization with plasma membrane (white), plasma membrane together with vesicular puncta (gray), and vesicular expression (black). The second bar represents the percentage of embryos presenting defective embryogenesis (light green) and hyperfusion (dark green). Most *rab-5*(*RNAi*) and *dyn-1*(*RNAi*) embryos arrest at early embryogenesis before EFF-1 expression and before the time of hypodermal fusions (elongation/morphogenesis). Most embryos that escape the early arrest show hyperfusion and EFF-1 in apical plasma membranes. Mean of three independent experiments; n $\geq$ 20 embryos per experiment.

The scale bars represent 10 μm in (A), (B), and (F) and 2 μm in (E).

modest colocalization between EFF-1::GFP and DLG-1::RFP (Figures 2A and 2C). In contrast, in *rab-5*(*RNAi*), the intensity profile of EFF-1::GFP along a random line within the cell shows peaks overlapping with DLG-1::RFP peaks (Figure 2D), confirming the visual observation of enrichment of EFF-1 on apical junctions. Thus, EFF-1 is not present in apical cell membranes in the steady state. The overall level of EFF-1 was not changed; the average EFF-1::GFP intensity in control RNAi (70 ± 23 gray values/pixel; 17 cells from ten embryos) was similar to EFF-1::GFP intensity after *rab-5* RNAi (69 ± 10 gray values/pixel; 23 cells from eight embryos). Our data suggest that, when *rab-5* activity is reduced, EFF-1::GFP redistributes from intracellular vesicles to the plasma membranes.

To determine the effect of *rab-5* knockdown on the dynamics of EFF-1 at the plasma membrane during fusion, we followed EFF-1::GFP colocalization with the apical plasma

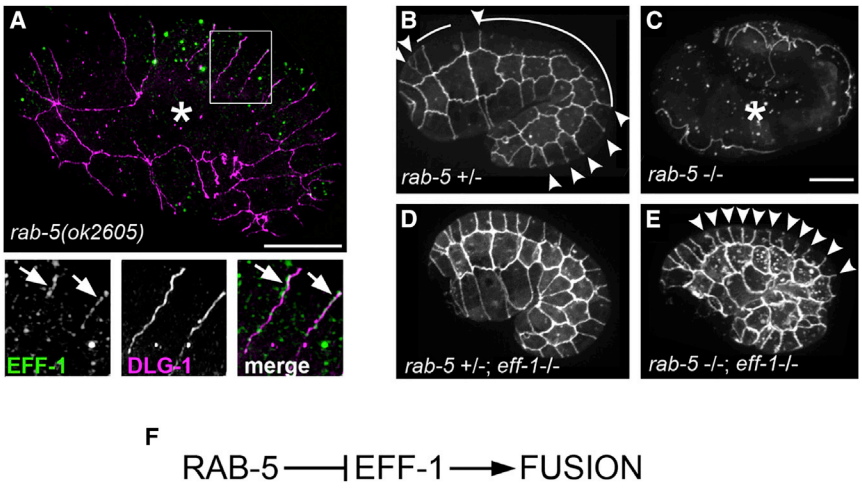

Figure 3. Loss of *rab-5* Function Induces *eff-1*-Mediated Ectopic Fusion

(A) Ectopic fusion (asterisk) and EFF-1 mislocalization to the plasma membrane (arrows) caused by *rab-5*(*ok2605*). Immunofluorescence with anti-EFF-1 (green) and anti-DLG-1 antibody (magenta) followed by SIM is shown. Magnifications of the inset region represent EFF-1 and DLG-1 fluorescence in separate channels and merged.

(B–E) Epistasis analysis between *rab-5* and *eff-1* reveals *rab-5* as a negative regulator of *eff-1*. Fusion pattern was visualized by live imaging of junction marker DLG-1::RFP expressed in *rab-5* and *eff-1* single and double mutants.

(B) Heterozygous *rab-5* mutant exhibits wild-type fusion. Fused cells are outlined with white stroke, junctions that will fuse later in embryogenesis (arrowheads).

(C) Hyperfusion induced by *rab-5* homozygous mutation is shown (asterisk).

(D) No fusion in double *rab-5*(+/−); *eff-1*(−/−) mutant is shown.

(E) Fusion is blocked in double *rab-5*(−/−); *eff-1*(−/−) mutant, unfused junctions (arrowheads).

(F) Scheme of RAB-5-negative regulation of EFF-1 derived from the epistasis analysis. The scale bars represent 10 μm.

membrane using the DLG-1::RFP reporter protein. We found that, when the apical junctions begin to disassemble in *rab-5* RNAi embryos, EFF-1 is still weakly detected on cell membranes (Figure 2E, arrowhead, time 0'; Movie S3), but after 10 min of apical junction disassembly, EFF-1::GFP cannot be detected where the plasma membrane used to be (Figure 2E, arrowhead). Taken together, our results show that reduction in RAB-5 activity stabilizes EFF-1 localization at the apical plasma membrane of fusing cells, suggesting that RAB-5 is involved in the uptake of EFF-1 from the apical plasma membrane to endosomes.

To independently determine whether EFF-1 is indeed removed from the plasma membrane by endocytosis, we depleted a central endocytosis regulator, dynamin. DYN-1 is the only dynamin in *C. elegans* and is essential for embryogenesis (Clark et al., 1997). Significantly, in all surviving embryos that developed to the morphogenesis stages when fusion occurs (Figure 1), *dyn-1* RNAi induced EFF-1::GFP mislocalization to the apical membrane of hypodermal cells (Figures 2F, 2G, and S2; Movie S5). These results support the hypothesis that EFF-1 localizes to endosomal organelles in the steady state. However, during embryonic morphogenesis, EFF-1 is continuously recycling between the apical plasma membrane and the endolysosomal system via receptor-mediated endocytosis. When internalization is blocked, EFF-1 mislocalizes to the apical plasma membrane.

RAB-5 and DYN-1 Control Cell Fusion

dyn-1 and *rab*-5 knockdown results in early embryonic arrest. Because most embryos arrest before EFF-1 expression and morphogenesis, we analyzed embryos that escape early arrest. *dyn-1* RNAi treatments showed defects associated with ectopic fusion in 10%–20% of all the embryos (Figure 2G). The *dyn-1* RNAi-induced hyperfusion phenotype was not observed in *eff-1*(*hy21*) embryos that lost the extrachromosomal EFF-1::GFP (n ~ 100), demonstrating that ectopic fusion observed following dynamin downregulation is mediated by EFF-1, indicating that *eff-1* is epistatic to *dyn-1*.

Like with *dyn-1*(*RNAi*), in *rab-5*(*ok2605*)-null mutant, endogenous EFF-1 was mislocalized to apical junctions (Figure 3A), consistent with the *rab-5* RNAi effect on EFF-1::GFP localization (Figures 2D and 2E). Moreover, we found that 20% of the *rab-5*(*ok2605*) embryos that escape early lethality showed ectopic fusion phenotype (n = 35; Figure 3A, asterisk).

To find out whether the hyperfusion phenotype induced by *rab-5* knockdown depends on *eff-1* activity, we followed the fusion phenotype of double *eff-1*;*rab-5* mutants. *rab-5* heterozygous embryos showed normal fusion pattern (Figure 3B). In contrast, we observed excessive fusion in *rab-5* homozygous embryos (Figure 3C, asterisk). We found that *eff-1*(*hy21*) mutants displayed suppressed cell fusion in both *rab-5* hetero- and homozygous embryos (Figures 3D and 3E). Thus, *eff-1* is epistatic to *rab-5*, suggesting that the hyperfusion induced by the deletion of *rab-5* is *eff-1* dependent. In other words, *rab-5* inhibits the fusion-inducing activity of *eff-1* (Figure 3F). We conclude that downregulation of dynamin or RAB-5 results in an increase in EFF-1 localization to the apical plasma membrane and hyperfusion in embryos that did not arrest early in embryogenesis (Figures 2 and S2).

To identify additional genes responsible for intracellular EFF-1 trafficking, localization, and function, we screened candidate genes for defects in cell fusion and EFF-1 localization using immunofluorescence and live imaging. Most trafficking mutants tested did not show differences compared with wild-type animals (Tables S2 and S3). As previously shown by Kontani et al. (2005), mutations in the vacuolar ATPase complex proteins caused hyperfusion in late stages of embryonic morphogenesis (Figure S3). Because mutations in the V-ATPase complex affect multiple endocytic trafficking pathways (Nishi and Forgac, 2002) and exocytosis of multivesicular bodies (Liégeois et al., 2006), it is difficult to distinguish which trafficking stages were involved in EFF-1-retarded hyperfusion.

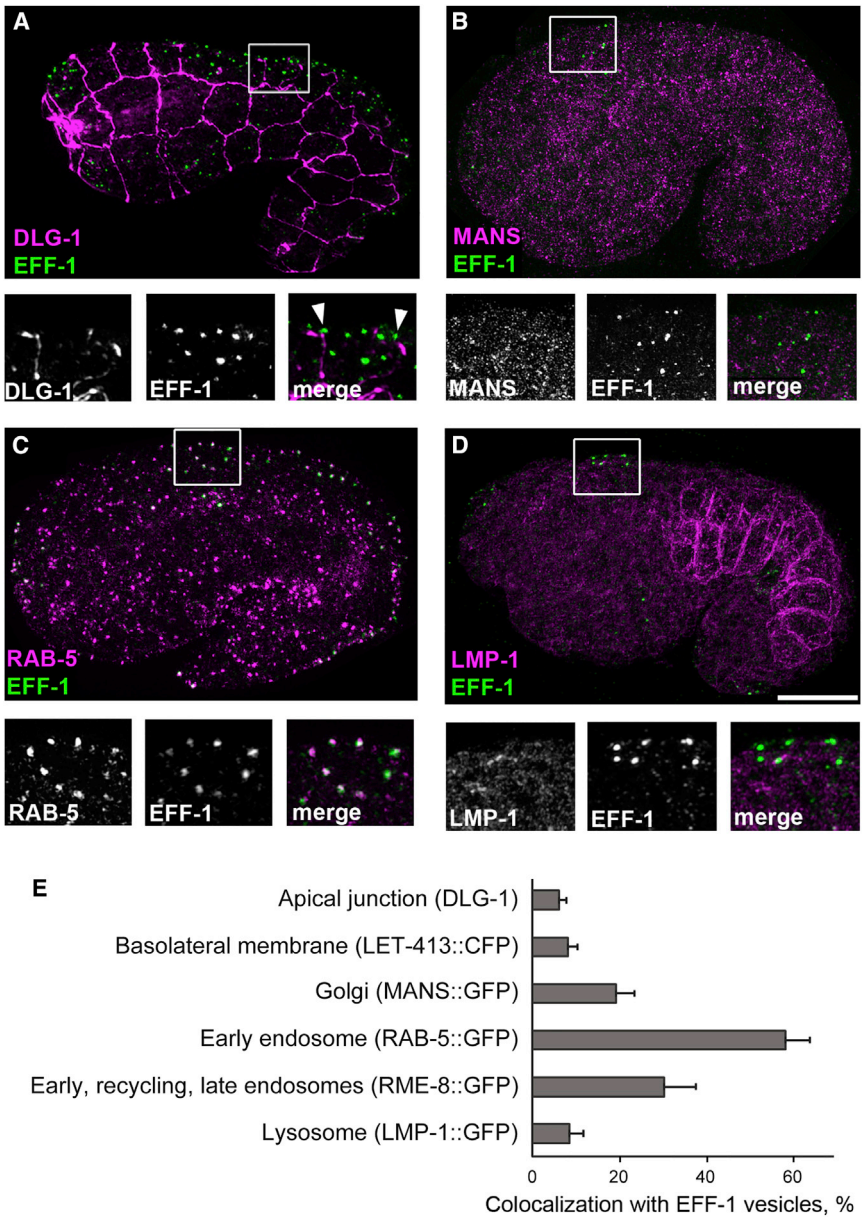

Figure 4. EFF-1 Localization to Intracellular Compartments

(A) The localization of EFF-1 revealed by an anti-EFF-1 monoclonal antibody (green) is compared with the apical junction (anti-DLG-1 antibody, magenta) using superresolution microscopy (SIM). (B–D) EFF-1 colocalization with stably expressed GFP-tagged markers of different membrane-bound organelles, detected with anti-GFP antibodies, magenta: Golgi complex, MANS::GFP (B); early endosomes, RAB-5::GFP (C), and lysosomes, LMP-1::GFP (D). Lower panel represents inset areas enlarged and shown in separate channels and merged.

(E) Quantification of EFF-1 colocalization with different markers represents the ratio of EFF-1 puncta that overlay the puncta of indicated marker (number of colocalized EFF-1 puncta/total number of EFF-1 puncta as percentage). Bars represent mean percentage of colocalization calculated in 5–20 embryos (100–1,000 cells) ± SEM. The colocalization above 5% is shown in the graph. The full list of intracellular markers tested, number of puncta, and number of embryos per marker are shown in Table S1. See also Figure S4. The scale bar represents 10 μm.

EFF-1 Localizes to Early Endosomes

To identify the puncta where EFF-1 localizes, we performed colocalization studies using structured illumination microscopy (SIM). *C. elegans* embryos that express GFP-tagged cellular markers were immunostained with anti-GFP antibody to detect intracellular membrane compartments and with anti-EFF-1 antibody to localize endogenous EFF-1. Colocalization was quantified as percentage of endogenous EFF-1 puncta that overlapped with each of the anti-GFP antibodies on superresolution 3D images (see Experimental Procedures). Only 6% of EFF-1 puncta were localized to the region of apical junctions, whereas 13% were associated with apical junctions within 200 nm distance (Figure 4A). EFF-1 was enriched in structures that were positive for the early endosome marker RAB-5::GFP (58% of colocalization; n = 21 embryos; Figures 4C and 4E; Table S1). Thirty percent of EFF-1 puncta colocalized with the general endosomal marker RME-8 (early, late endosome, and multivesicular body; Figures 4E, S4E, and S4F; Table S1), supporting EFF-1 presence in RAB-5-positive early endosomes. EFF-1 also showed significant colocalization with the Golgi marker MANS::GFP (19%), possibly due to secretory sorting and recycling between endosomes and the Golgi (Figures 4B and 4E). Nine percent of EFF-1 puncta colocalized with the lysosomal marker LMP-1::GFP (Figures 4D and 4E), suggesting that EFF-1 is also transported to lysosomes where it is probably degraded. EFF-1 puncta colocalized less than 5% with most other markers examined (RAB-10::GFP, RME-1::GFP, RAB-11::GFP, RAB-7::GFP, ALX-1::GFP, LGG-1::GFP, and VHA-5::GFP; Table S1). Data sets for these markers were not statistically different from each other and probably represent the background of the measurements. Thus, wild-type endogenous EFF-1 is detected mainly in RAB-5 early endosomes and is only transiently associated with the apical domains of the plasma membrane where it acts to fuse cells.

We found that, in a mixed population of embryos expressing EFF-1, 58% of the puncta colocalized with RAB-5 (Figure 4E). To determine whether EFF-1/RAB-5 colocalization changes over time of fusion, we measured their colocalization during

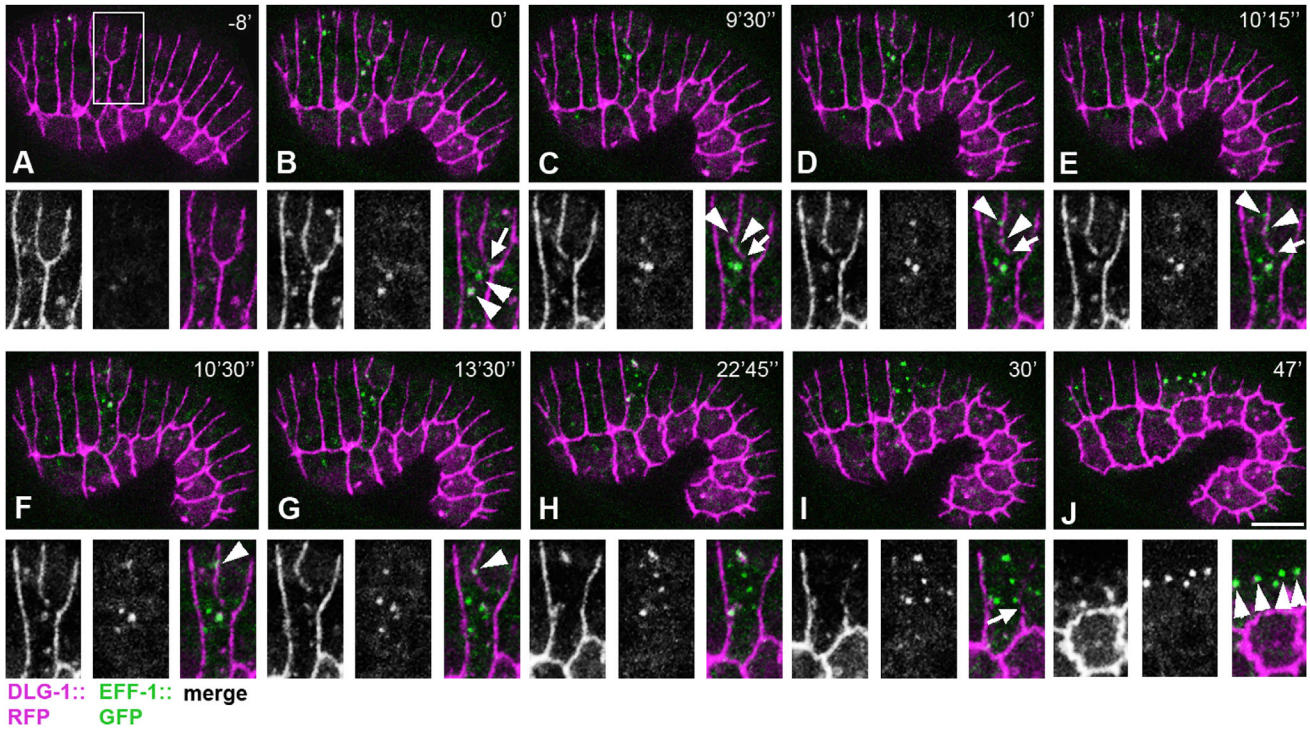

Figure 5. The Dynamics of EFF-1::GFP during Cell Fusion

Live imaging of EFF-1::GFP (green) and apical junction marker DLG-1::RFP (magenta) in the process of dorsal fusions. Fusing cells are highlighted in (A), and higher magnification inset is shown below in separate channels: DLG-1::RFP (left); EFF-1::GFP (middle); and merged image (right panel). (B–E) Early stages of apical junction disassembly (arrows). Dynamic colocalization of EFF-1 and DLG-1 on plasma membranes (arrowheads). Time points (in minutes and seconds) of image acquisition are presented in the upper right corners. Time 0' indicates the beginning of Movie S1.

(A) EFF-1::GFP fluorescence is barely detectable in cells that are going to fuse.

(B) EFF-1::GFP appears in the cell cytoplasm within a pair of bright vesicles (arrowheads) and diffuse where the cell junction disassembles (arrow).

(C–E) EFF-1::GFP arrives at the cell junction from both fusing cells (C, arrowheads) and move along the junction (D and E, arrowheads). Arrows mark the edge of the cell junction undergoing disassembly.

(F) EFF-1 puncta coming from opposite cells join together on the cell junction (arrowhead).

(G and H) At the end of the first dorsal cell fusion, EFF-1::GFP puncta are distributed in the cytoplasm of the syncytium.

(I) Second junction discontinuity revealing the second cell fusion (arrow).

(J) EFF-1::GFP vesicles become larger, brighter, and aligned in an anterior-posterior line (arrowheads) within the intermediate syncytium. The scale bar represents 10 μm.

See Movies S1 and S2.

distinct stages in embryonic morphogenesis. When hypodermal cell fusions are in progress (1.5-fold stage of elongation), we found that 45% of EFF-1 puncta colocalize with RAB-5 (n = 12; Figure S4A). Colocalization increased and reached a maximum when most dorsal cell fusions have been completed (69%; 1.8-fold stage; n = 18; Figure S4B). At later stages, we found a gradual reduction in EFF-1 colocalization with RAB-5 (Figures S4C and S4D). In contrast, colocalization of EFF-1 with lysosomal LMP-1 increased from 8% at the 1.5-fold stage to 26% at the 2-fold stage when most epidermal fusions have been completed. To summarize, we observe only minor localization of EFF-1 at the apical and basolateral membranes; rather, most EFF-1 localizes to early endosomes, the endocytic pathway, and to the Golgi apparatus. After cells fuse, most of EFF-1 is localized to RAB-5-positive early endosomes and partially in lysosomes where EFF-1 may undergo degradation.

EFF-1 Shuttles to the Fusion Sites and Back to the Cell Interior within Vesicles

To determine whether wild-type EFF-1::GFP transiently shuttles to the plasma membrane and back to the intracellular early endosomes, we analyzed time-lapse movies. Followed by live imaging, EFF-1::GFP appeared dispersed in the cytoplasm within puncta in hypodermal cells ready to fuse (Figure 5B). Faint EFF-1::GFP puncta approached the cell junctions marked by DLG-1::RFP from both fusing cells transiently (Figures 5C–5E, arrowheads). About 10% of EFF-1::GFP puncta oscillated within 0.5 μm from the cell junction for 15 ± 6 min (n = 20 EFF-1::GFP puncta from eight embryos; Figures 5C–5G, arrowheads; Movies S1 and S2). During this time, 80% of the observed apical junctions began to disassemble (n = 20; Figures 5B–5E, arrows) to complete syncytia formation. The number of EFF-1::GFP-positive puncta increased during the process of cell fusion (Figures 5C–5I). After disassembly

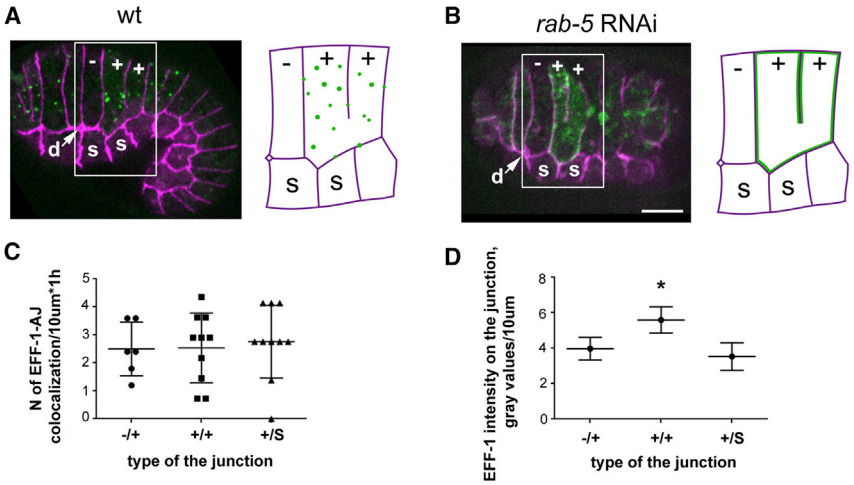

Figure 6. EFF-1 Is Constitutively Transported to All Apical Plasma Membrane Domains

(A) EFF-1::GFP (green) puncta colocalization with the apical junctions marked DLG-1::RFP (magenta). On the picture and on the schematics, EFF-1-expressing cells are marked with "+," epidermal cell that does not express EFF-1 is marked by "−"; d, deirid; s, seam cell. EFF-1::GFP is transiently localized to the junctions between different cell types: −/+; +/+; and +/s. Schematics represent highlighted cells from the picture; EFF-1::GFP (green puncta) transiently colocalizes with apical junctions (see Movie S2).

(B) After *rab-5(RNAi)*, EFF-1::GFP is spread to all the junctions of −/+, +/+, and +/s types. In schematics, accumulation of EFF-1::GFP is visualized by the green line on the magenta apical junctions (see Movie S6).

(C) Categorical scatterplot of EFF-1::GFP vesicle colocalization to the different junctions per 10 μm of junction length per hour, measured in wild-type embryos. Each point represents number of events (colocalization) per junction over time. n = 8 embryos with a total of 6–10 junctions analyzed over ~50 min. Middle line reflects the mean; upper and lower lines show SD. Thus, EFF-1-containing vesicles transiently associate (e.g., fuse) to all types of junctions. There is no statistical difference between data sets (Student's t test).

(D) EFF-1::GFP relative intensity measured on the cell junctions in embryos treated with *rab-5(RNAi)*. Five junctions of each type over ten time points were analyzed (n = 50); movies of three independent embryos were used (normalized to EFF-1::GFP gray values × 10^3/10 μm). Data are presented as mean (middle line) ± SD (upper and lower lines). There is no difference between intensities measured on −/+ and on +/s junction. *$p < 0.05$ (Student's t test).

of the apical junctions, small EFF-1::GFP puncta merged into larger and brighter puncta (Figure 5J, arrowheads). Based on these findings, we hypothesize that EFF-1 is stored within early endosomes and is transiently transported to the cell surface when cells are ready to fuse.

EFF-1 Is Dynamically Delivered to All Apical Domains, Including Ones that Do Not Fuse

It has previously been reported that EFF-1*::GFP (*, mutant protein; del Campo et al., 2005) accumulates only at the membranes between cells that are destined to fuse. However, the dynamic subcellular localization of EFF-1*::GFP does not match our observations made by immunofluorescence staining using anti-EFF-1 monoclonal antibodies (Figures 1 and S5) and our EFF-1::GFP dynamic behavior (Figure 5; Movies S1 and S2). Furthermore, the EFF-1*::GFP construct harbors two point mutations at highly conserved sites, T176A and N529D, and does not rescue *eff-1(hy21)* animals (Avinoam and Podbilewicz, 2011).

To test whether EFF-1 transport is specifically targeted to the plasma membrane domains where fusion occurs, we analyzed the directionality of EFF-1::GFP delivery to the apical junctions between the cells, which lie posterior to the deirid (d) (Figure 6A). In these examples, a dorsal hypodermal cell that is not expressing EFF-1::GFP at a given time point is marked by minus; the adjacent dorsal and posterior cells express EFF-1::GFP and are marked with plus; seam cells are marked with the letter "s". We found that EFF-1::GFP is transiently localized to all apical plasma membrane domains in "+" cells (Figure 6A; Movie S5). There is no statistical difference between the number of EFF-1::GFP puncta transiently localized between EFF-1(+) and EFF-1(−), between two EFF-1s(+/+), and the junction between EFF-1/seam cells (+/s; Figure 6C). Thus, in contrast to the previous paradigm (del Campo et al., 2005), we found that EFF-1 is continuously and dynamically localizing to all apical plasma membrane domains and not only to those destined to fuse.

If EFF-1 is constitutively and nonspecifically internalized via receptor-mediated endocytosis from all plasma membrane domains, then following RAB-5(RNAi), EFF-1::GFP may be mislocalized to all apical domains and not only to the junctions destined to fuse. We found that EFF-1 transport to the plasma membrane was not affected whereas EFF-1 endocytosis was blocked by RAB-5(RNAi). As a result, EFF-1 was localized at all the apical plasma membrane domains of the + cells (Figure 6B; Movie S6). We then measured the intensities of EFF-1::GFP at the junctions between −/+ and +/s junctions. We found that the relative EFF-1::GFP intensities on the −/+ and +/s junctions are not statistically different (Figure 6D). For the membranes between two EFF-1-expressing cells (+/+), the intensity of EFF-1::GFP was higher, but this is to be expected as both cells contribute EFF-1 to this junction (Figure 6D). Thus, we show that EFF-1 transport to and from the plasma membrane has no specificity according to the junction type and the place of fusion. Based on our results, we propose that vesicles containing EFF-1::GFP cargo have the same probability of fusing with all apical plasma membranes.

In summary, EFF-1 localization in *C. elegans* embryonic epidermal cells is tightly maintained in early endosomes by the RAB-5- and DYN-1-dependent endocytic machinery. The EFF-1 protein is dynamically delivered to all apical plasma membranes transiently and without specificity to the place of fusion.

DISCUSSION

Based on our results, we propose a model for the regulation of EFF-1 localization and fusion activity by endocytosis.

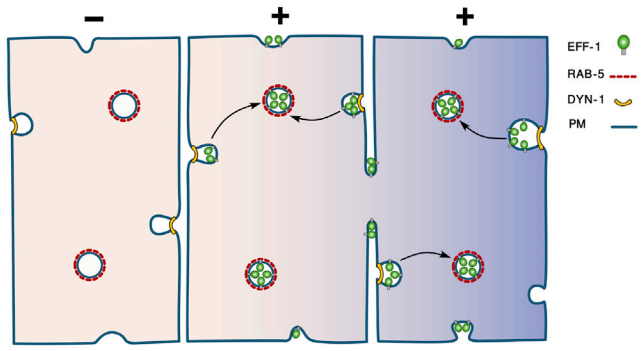

Figure 7. Model of Cell Fusion in *C. elegans* Embryonic Hypodermis
EFF-1 (green) is expressed in all surrounding plasma membranes (blue line) without relation to the future fusion-fated membranes. Cell that does not express EFF-1 (–) is colored in light khaki (left cell); fusion-fated cells that express EFF-1 (+) are colored in gradient of purple to khaki (central and right cells). The excess EFF-1 is actively removed from the cell surface via endocytosis in a dynamin- (yellow line) and RAB-5- (red dashed line) dependent mechanism. EFF-1 accumulates in the cytoplasm within early endosomes (circles outlined with the red dashed line). Only when EFF-1 is simultaneously present in both neighboring membranes, cell fusion is activated.

Synthesized EFF-1 transiently localizes to the surrounding apical plasma membranes of EFF-1-expressing cells. Membrane fusion is activated when the concentration of EFF-1 on two opposing membranes exceed a certain threshold and is mediated by homotypic interactions between EFF-1 proteins expressed from two cells (Podbilewicz et al., 2006). After constitutive non-selective targeting to all the apical domains of the plasma membrane, EFF-1 is recycled to early endosomes via dynamin/RAB-5-mediated trafficking (Figure 7). EFF-1 accumulates in RAB-5-positive endosomes probably because the rate of internalization is faster than the rate of transport to the apical plasma membranes. If EFF-1 trafficking is disrupted by RAB-5 knockdown or by DYN-1 downregulation, EFF-1 accumulates in the plasma membranes and can cause excessive cell fusion that contributes to embryonic lethality during elongation (morphogenesis).

Traffic Defects May Cause EFF-1 Membrane Accumulation Prior to Fusion

Our results demonstrate that cell-cell fusion in *C. elegans* embryos requires transient and low level of EFF-1 localization to the fusing cell membranes (Figures S5A–S5D). In contrast to the results reported here, EFF-1 stable expression at the plasma membrane was observed in previous studies (Avinoam et al., 2011; del Campo et al., 2005). Indeed, an EFF-1*::GFP was concentrated at cell-cell apical junctions in *C. elegans* embryos (Figure S5E, arrow; del Campo et al., 2005). However, we found that this EFF-1*::GFP reporter carries two point mutations (T176A and N529D) and does not rescue *eff-1*(*hy21*) animals (Avinoam and Podbilewicz, 2011). We suggest that the mutations cause EFF-1*::GFP abnormal accumulation in some apical junctions. Additionally, EFF-1 ectopically expressed under a heat shock promoter was detected at the plasma membranes of intestinal cells just before fusion in *C. elegans* embryos (Figure S5F, arrows). This was also true for EFF-1 that was ectopically expressed in nematode neurons, cultured insect, and mammalian cells (Figure S5G, arrows; Avinoam et al., 2011; Neumann et al., 2015; Podbilewicz et al., 2006; Zeev-Ben-Mordehai et al., 2014). These ectopic overexpression setups give rise to aberrant distribution of EFF-1 that does not mirror that of the highly regulated endogenous protein in the embryonic epidermis.

EFF-1 Fuses Cells Locally

According to the homotypic fusion model supported by recent biochemical and structural evidence, membrane fusion is mediated by EFF-1 trans-trimerization (Pérez-Vargas et al., 2014). The bright EFF-1 intracellular vesicles detected by immunofluorescence are likely to be composed of EFF-1 in a postfusion, trimeric conformation. It is unlikely that the different anti-EFF-1 antibodies we have used are trimer specific, because the same pattern was observed by EFF-1::GFP expression. Moreover, our monoclonal antibodies equally recognize both monomers and trimers by ELISA and western blot, including in samples of purified monomeric and trimeric EFF-1 ectodomains (data not shown). EFF-1::GFP vesicles became visible only at the onset of membrane fusion (within minutes before junction disassembly). We suggest that the concentration of EFF-1 monomers that is sufficient to initiate membrane fusion in vivo is low and barely detectable by confocal and superresolution microscopy. Localized high concentrations of EFF-1 monomers may be sufficient to initiate trans-EFF-1 complex formation and fusion.

EFF-1 vesicles are concentrated along lines that run parallel to the seam cells and are enriched with microtubules (Figure S1). We also observed that junction disassembly is often initiated at specific locations within cell junctions. These findings are compatible with the idea that microtubules mediate EFF-1 transport to specific places on the cell membranes from both cells undergoing fusion. EFF-1 local enrichment on both sides of the plasma membranes is sufficient to initiate cell fusion, as supported by genetic mosaic analyses of EFF-1-mediated fusion in *C. elegans*, in cell culture, and between viruses and cells (Avinoam et al., 2011; Podbilewicz et al., 2006).

EFF-1 Trafficking Is Regulated by RAB-5

Endocytosis plays an essential role in intercellular signaling, uptake of nutrients, and membrane recycling (Grant and Donaldson, 2009; McMahon and Boucrot, 2011; Mellman, 1996). RAB-5 is a central regulator of the early endocytic pathway and is a marker for the early endosome (Mizuno-Yamasaki et al., 2012; Sato et al., 2014; Zerial and McBride, 2001). Based on live imaging and immunolocalization, we propose that EFF-1 is transiently localized to the plasma membrane, internalized, and transported to early endosomes (Figure 7). There are two possibilities for how EFF-1 is transported from the plasma membrane to the early endosome. Some cells completely internalize their plasma membrane within 0.5–2 hr (Steinman et al., 1976), and EFF-1 can be endocytosed with the general membrane turnover. Another option is that EFF-1 transport is specific and mediated by an endocytosis signal (Traub, 2009). Trans-oligomerization of EFF-1 from opposing plasma membranes and the following conformational changes of trimers are proposed to dock the membranes and to initiate membrane fusion

(Pérez-Vargas et al., 2014). Soluble DIII was shown to block EFF-1-mediated cell fusion in transfected mammalian cells, supporting the model based on class II viral fusion proteins in which DIII translocation from a linear pre-fusion conformation to a parallel postfusion hairpin conformation is required for membrane fusion (Pérez-Vargas et al., 2014). The localization of EFF-1::GFP in *rab-5*(RNAi) embryos shows mislocalization to all the apical plasma membranes including the domains that do not normally fuse (Figures 2B and 6B). Thus, EFF-1 is transported to all apical plasma membranes domains and not only to fusion-fated domains of the apical plasma membrane.

Is Endocytosis a Universal Regulator of Cell Fusion?

Because EFF-1 is a powerful fusogen, specialized safety mechanisms are required to prevent ectopic cell fusion. First, EFF-1 expression is regulated transcriptionally (Alper and Kenyon, 2002; Brabin et al., 2011; Cassata et al., 2005; Fernandes and Sternberg, 2007; Margalit et al., 2007; Mason et al., 2008; Pellegrino et al., 2011; Rasmussen et al., 2008; Shemer and Podbilewicz, 2002; Walser et al., 2006; Weinstein and Mendoza, 2013; Yi and Sommer, 2007). Gene-expression-based regulation may be the primary mechanism of specificity in EFF-1-mediated fusion. Second, EFF-1 expressed in one cell needs a partner from a neighboring cell in order to mediate fusion (Podbilewicz et al., 2006). Third, local concentration of EFF-1 on the plasma membrane is downregulated by dynamin/RAB-5-mediated endocytosis. Trafficking of EFF-1 may provide a fine-tuning to its fusion activity. During mammalian myoblast and osteoclast fusion, the opposite control mechanism was found to occur: cells required endocytosis and dynamin activity in order to fuse (Leikina et al., 2013; Shin et al., 2014; Verma et al., 2014). It is conceivable that endocytosis and recycling act during diverse cell-cell fusion events. Recently, the engulfment pathway was shown to act upstream of EFF-1 activity during regenerative axonal fusion in *C. elegans* (Neumann et al., 2015). In addition, gamete fusion in the mouse was linked to endocytosis and exocytosis (Satouh et al., 2012; Wassarman and Litscher, 2008). In *Drosophila* myoblast fusion, the adhesion molecule SNS, which is essential for fusion, was shown to colocalize with Rab-5 (Haralalka et al., 2014). Here, we found a clear case in which endocytosis negatively regulates EFF-1-mediated cell-cell fusion to prevent excessive syncytia formation, which can result in abnormalities and contributes to late embryonic lethality.

In conclusion, we found that the GTPases RAB-5 and dynamin control EFF-1 transient localization on the surface of cells destined to fuse and prevent excess fusion by dynamically and constitutively internalizing this fusion protein from all the apical domains of the plasma membrane.

EXPERIMENTAL PROCEDURES

Strains and Transgenic Animals

All nematode strains were maintained according to standard protocols (Brenner, 1974). The list of *C. elegans* strains used in this study is in Tables S1 and S2 and Supplemental Experimental Procedures. For the construction of *eff-1*::*gfp* rescue strain, germline transformation was performed using standard protocols (Mello and Fire, 1995). *eff-1*::*gfp* fosmid was ordered from Transgenome (Sarov et al., 2012) and was injected into BP953 (*eff-1*(*hy21*)*II*; *mcIs46* [*dlg-1*::*RFP*]; Diogon et al., 2007) at 50 ng/μl concentration. Transgenic lines were kept as extrachromosomal arrays and maintained by following the rescue phenotype of *eff-1*(*hy21ts*) at 25°C.

Immunofluorescence

Embryos were prepared for immunostaining as described in Supplemental Experimental Procedures. The following primary antibodies were used at the dilutions indicated: α-EFF-1 (mouse ascites 20.10 and 10.5; 1:1,000); MH27 (α-AJM-1; mouse; 1:500); α-GFP (rabbit; 1:500; MBL); and α-tubulin (mouse; Sigma; 1:500). α-DLG-1 antibody (rabbit; 1:400) was a kind gift from Prof. Dr. Olaf Bossinger (RWTH Aachen University). MH46 (α-myotactin; mouse; 1:400; Hresko et al., 1994) was a kind gift from Dr. Limor Broday (Tel Aviv University); mouse monoclonal antibodies against *C. elegans* proteins DYN-1, CYP33E1, PAS-7, and HSP60 were obtained from Developmental Studies Hybridoma Bank and used at 1:10 dilution. Texas Red-X phalloidin (Molecular Probes) at a final concentration of 0.2 μM was added with the secondary antibody.

Anti-EFF-1 Antibody Production

Anti-EFF-1 antibodies were prepared against purified EFF-1EC obtained as described (Pérez-Vargas et al., 2014), and the hybridomas were prepared and screened by ELISA in the lab of Africa Gonzalez (Vigo University). 20.10 and 10.5 ascites were used for immunostaining of *C. elegans* embryos and larvae (Fridman, 2012).

Microscopy and Live Imaging

Images of fixed samples were taken on Zeiss LSM 700 confocal microscope with X63/1.4 PlanApo objective. Superresolution images were obtained using Elyra S.1 structured illumination system (SIM) with X63/1.4 PlanApo objective and EMCCD iXon camera (Andor). Confocal or SIM z stacks were analyzed and processed by Zen software (Zeiss).

For the imaging of live embryos, gravid adult hermaphrodites were dissected in 50 μl of 0.7× egg salts and embryos were moved to 2% agar pad with a mouth pipette. The specimen was covered with a coverslip (1.5H) and sealed with scotch tape to prevent drying. Images were acquired using spinning disc Revolution XD confocal system (Andor) based on Nikon Eclipse Ti microscope equipped with 100×/1.3 PlanFluor objective, perfect focus system; CSU-X1 spinning disc (Yokogawa) and iXon3 EMCCD camera (Andor) operated by IQ2 software (Andor). Image sequences were further processed and analyzed with ImageJ (NIH). Figures were prepared using Adobe Photoshop CS5 and Adobe Illustrator CS11.

Quantitation of Colocalization and Statistics

Colocalization was quantified manually on individual z slices (~100 per embryo), analyzing red and green channels separately on superresolution SIM images using Zen software (Zeiss). Colocalization analysis of EFF-1 puncta was performed on embryos carrying the GFP-tagged protein of interest labeled with antibodies against GFP (Alexa 488; green channel) and with monoclonal antibodies against EFF-1 (Alexa Fluor 568; red channel). EFF-1 puncta were considered colocalized with puncta containing GFP marker if the areas of those puncta showed more than 50% overlay. The percentage of colocalization is expressed as the ratio of puncta positive for EFF-1 and GFP out of the total number of EFF-1 puncta in the embryonic hypodermis. For each marker, at least five embryos were quantified; data are shown as mean ± SEM (see Table S1). Significant differences between two groups of measurements were determined by the two-tailed unpaired t test using Excel. For statistical comparison of multiple groups, we used ANOVA test in Excel.

RNAi

RNAi by feeding was performed with an ORF-RNAi library (Rual et al., 2004). RNAi feeding protocol was used (Beifuss and Gumienny, 2012). We used *dyn-1*, *rab-5*, *rabx-5*, and *rme-6* RNAi, *bli-4* was used as a positive control and C06C3.5 as a negative control. For each clone, 5 ml LB media containing 50 μg/ml carbenicillin (Sigma) was inoculated with a single colony and incubated overnight at 37°C at 220 rpm. dsRNA production was induced by adding 1 mM IPTG (Sigma) to the cultures and additional incubation for 4 hr. Each bacterial culture (50 μl) was inoculated into NGM RNAi plate containing 50 μg/ml carbenicillin and 1 mM IPTG and dried. *C. elegans* L4 stage was isolated to

NGM plates for 1 hr to get rid of OP50 bacteria in the intestine. Embryos were examined on the next day after larvae were transferred to plates with bacteria producing the specific dsRNAs.

SUPPLEMENTAL INFORMATION

Supplemental Information includes Supplemental Experimental Procedures, five figures, three tables, and six movies and can be found with this article online at http://dx.doi.org/10.1016/j.celrep.2016.01.027.

AUTHOR CONTRIBUTIONS

K.S. performed the experiments. B.P. did initial SIM experiments. K.S. and B.P. conceived the project, analyzed the data, and wrote the manuscript.

ACKNOWLEDGMENTS

We thank B. Grant, O. Bossinger, M. Labouesse, B. Mohler, Z. Hong, A. Chisholm, and L. Broday for *C. elegans* strains. We acknowledge CGC (NIH Office of Research Infrastructure Programs P40 OD010440) and *C. elegans* knockout consortium for strains. We thank TransgenOme for *eff-1p*::*eff-1*::*gfp* fosmid; A. Gonzalez, O. Bossinger, L. Broday, and Developmental Studies Hybridoma Bank (U. of Iowa) for antibodies; C. Valansi for initial characterization of antibodies against EFF-1; O. Avinoam, D. Cassel, M. Hilliard, M. Oren-Suissa, and E. Schejter for critically reading the manuscript; and T. Rapoport and members of his lab for discussions. B.P. was a Grass fellow at Radcliffe Institute for Advanced Study at Harvard. K.S. was supported by the Ministry of Absorption, Israel (N061486). The work was funded by European Research Council (ERC) advanced grant 268843, GIF German-Israeli Foundation for Scientific Research and Development (grant 937/2006), US-Israel Binational Science Foundation (grant 2013151), and the Israel Science Foundation grant 443/12.

Received: March 16, 2015
Revised: November 30, 2015
Accepted: January 4, 2016
Published: February 4, 2016

REFERENCES

Aguilar, P.S., Baylies, M.K., Fleissner, A., Helming, L., Inoue, N., Podbilewicz, B., Wang, H., and Wong, M. (2013). Genetic basis of cell-cell fusion mechanisms. Trends Genet. *29*, 427–437.

Alper, S., and Kenyon, C. (2002). The zinc finger protein REF-2 functions with the Hox genes to inhibit cell fusion in the ventral epidermis of *C. elegans*. Development *129*, 3335–3348.

Avinoam, O., and Podbilewicz, B. (2011). Eukaryotic cell-cell fusion families. Curr. Top. Membr. *68*, 209–234.

Avinoam, O., Fridman, K., Valansi, C., Abutbul, I., Zeev-Ben-Mordehai, T., Maurer, U.E., Sapir, A., Danino, D., Grünewald, K., White, J.M., and Podbilewicz, B. (2011). Conserved eukaryotic fusogens can fuse viral envelopes to cells. Science *332*, 589–592.

Beifuss, K.K., and Gumienny, T.L. (2012). RNAi screening to identify postembryonic phenotypes in C. elegans. J. Vis. Exp., e3442.

Brabin, C., Appleford, P.J., and Woollard, A. (2011). The Caenorhabditis elegans GATA factor ELT-1 works through the cell proliferation regulator BRO-1 and the Fusogen EFF-1 to maintain the seam stem-like fate. PLoS Genet. *7*, e1002200.

Brenner, S. (1974). The genetics of Caenorhabditis elegans. Genetics *77*, 71–94.

Cassata, G., Shemer, G., Morandi, P., Donhauser, R., Podbilewicz, B., and Baumeister, R. (2005). ceh-16/engrailed patterns the embryonic epidermis of Caenorhabditis elegans. Development *132*, 739–749.

Chen, C.C., Schweinsberg, P.J., Vashist, S., Mareiniss, D.P., Lambie, E.J., and Grant, B.D. (2006). RAB-10 is required for endocytic recycling in the Caenorhabditis elegans intestine. Mol. Biol. Cell *17*, 1286–1297.

Chen, E.H., Grote, E., Mohler, W., and Vignery, A. (2007). Cell-cell fusion. FEBS Lett. *581*, 2181–2193.

Clark, S.G., Shurland, D.L., Meyerowitz, E.M., Bargmann, C.I., and van der Bliek, A.M. (1997). A dynamin GTPase mutation causes a rapid and reversible temperature-inducible locomotion defect in C. elegans. Proc. Natl. Acad. Sci. USA *94*, 10438–10443.

del Campo, J.J., Opoku-Serebuoh, E., Isaacson, A.B., Scranton, V.L., Tucker, M., Han, M., and Mohler, W.A. (2005). Fusogenic activity of EFF-1 is regulated via dynamic localization in fusing somatic cells of C. elegans. Curr. Biol. *15*, 413–423.

Diogon, M., Wissler, F., Quintin, S., Nagamatsu, Y., Sookhareea, S., Landmann, F., Hutter, H., Vitale, N., and Labouesse, M. (2007). The RhoGAP RGA-2 and LET-502/ROCK achieve a balance of actomyosin-dependent forces in C. elegans epidermis to control morphogenesis. Development *134*, 2469–2479.

Fares, H., and Greenwald, I. (2001). Genetic analysis of endocytosis in Caenorhabditis elegans: coelomocyte uptake defective mutants. Genetics *159*, 133–145.

Fernandes, J.S., and Sternberg, P.W. (2007). The tailless ortholog nhr-67 regulates patterning of gene expression and morphogenesis in the C. elegans vulva. PLoS Genet. *3*, e69.

Fridman, K. (2012). Ultrastructure and function of AFF-1 and EFF-1 in membrane remodeling. MSc thesis (Haifa: Technion).

Gattegno, T., Mittal, A., Valansi, C., Nguyen, K.C., Hall, D.H., Chernomordik, L.V., and Podbilewicz, B. (2007). Genetic control of fusion pore expansion in the epidermis of Caenorhabditis elegans. Mol. Biol. Cell *18*, 1153–1166.

Grant, B., and Hirsh, D. (1999). Receptor-mediated endocytosis in the Caenorhabditis elegans oocyte. Mol. Biol. Cell *10*, 4311–4326.

Grant, B.D., and Donaldson, J.G. (2009). Pathways and mechanisms of endocytic recycling. Nat. Rev. Mol. Cell Biol. *10*, 597–608.

Haralalka, S., Shelton, C., Cartwright, H.N., Guo, F., Trimble, R., Kumar, R.P., and Abmayr, S.M. (2014). Live imaging provides new insights on dynamic F-actin filopodia and differential endocytosis during myoblast fusion in Drosophila. PLoS ONE *9*, e114126.

Hresko, M.C., Williams, B.D., and Waterston, R.H. (1994). Assembly of body wall muscle and muscle cell attachment structures in Caenorhabditis elegans. J. Cell Biol. *124*, 491–506.

Kim, J.H., Ren, Y., Ng, W.P., Li, S., Son, S., Kee, Y.S., Zhang, S., Zhang, G., Fletcher, D.A., Robinson, D.N., and Chen, E.H. (2015). Mechanical tension drives cell membrane fusion. Dev. Cell *32*, 561–573.

Kontani, K., Moskowitz, I.P., and Rothman, J.H. (2005). Repression of cell-cell fusion by components of the C. elegans vacuolar ATPase complex. Dev. Cell *8*, 787–794.

Kozlov, M.M., Campelo, F., Liska, N., Chernomordik, L.V., Marrink, S.J., and McMahon, H.T. (2014). Mechanisms shaping cell membranes. Curr. Opin. Cell Biol. *29*, 53–60.

Leikina, E., Melikov, K., Sanyal, S., Verma, S.K., Eun, B., Gebert, C., Pfeifer, K., Lizunov, V.A., Kozlov, M.M., and Chernomordik, L.V. (2013). Extracellular annexins and dynamin are important for sequential steps in myoblast fusion. J. Cell Biol. *200*, 109–123.

Liégeois, S., Benedetto, A., Garnier, J.M., Schwab, Y., and Labouesse, M. (2006). The V0-ATPase mediates apical secretion of exosomes containing Hedgehog-related proteins in Caenorhabditis elegans. J. Cell Biol. *173*, 949–961.

Losick, V.P., Fox, D.T., and Spradling, A.C. (2013). Polyploidization and cell fusion contribute to wound healing in the adult Drosophila epithelium. Curr. Biol. *23*, 2224–2232.

Luga, V., Zhang, L., Viloria-Petit, A.M., Ogunjimi, A.A., Inanlou, M.R., Chiu, E., Buchanan, M., Hosein, A.N., Basik, M., and Wrana, J.L. (2012). Exosomes

mediate stromal mobilization of autocrine Wnt-PCP signaling in breast cancer cell migration. Cell *151*, 1542–1556.

Margalit, A., Neufeld, E., Feinstein, N., Wilson, K.L., Podbilewicz, B., and Gruenbaum, Y. (2007). Barrier to autointegration factor blocks premature cell fusion and maintains adult muscle integrity in C. elegans. J. Cell Biol. *178*, 661–673.

Mason, D.A., Rabinowitz, J.S., and Portman, D.S. (2008). dmd-3, a doublesex-related gene regulated by tra-1, governs sex-specific morphogenesis in C. elegans. Development *135*, 2373–2382.

McMahon, H.T., and Boucrot, E. (2011). Molecular mechanism and physiological functions of clathrin-mediated endocytosis. Nat. Rev. Mol. Cell Biol. *12*, 517–533.

Medvinsky, A., and Smith, A. (2003). Stem cells: Fusion brings down barriers. Nature *422*, 823–825.

Mellman, I. (1996). Endocytosis and molecular sorting. Annu. Rev. Cell Dev. Biol. *12*, 575–625.

Mellman, I., and Yarden, Y. (2013). Endocytosis and cancer. Cold Spring Harb. Perspect. Biol. *5*, a016949.

Mello, C., and Fire, A. (1995). DNA transformation. In Methods in Cell Biology *Caenorhabditis elegans*: Model Biological Analysis of an Organism, H.F. Epstein and D.C. Shakes, eds. (San Diego: Academic Press), pp. 451–482.

Messa, M., Fernández-Busnadiego, R., Sun, E.W., Chen, H., Czapla, H., Wrasman, K., Wu, Y., Ko, G., Ross, T., Wendland, B., and De Camilli, P. (2014). Epsin deficiency impairs endocytosis by stalling the actin-dependent invagination of endocytic clathrin-coated pits. eLife *3*, e03311.

Mizuno-Yamasaki, E., Rivera-Molina, F., and Novick, P. (2012). GTPase networks in membrane traffic. Annu. Rev. Biochem. *81*, 637–659.

Mohler, W.A., Shemer, G., del Campo, J.J., Valansi, C., Opoku-Serebuoh, E., Scranton, V., Assaf, N., White, J.G., and Podbilewicz, B. (2002). The type I membrane protein EFF-1 is essential for developmental cell fusion. Dev. Cell *2*, 355–362.

Neumann, B., Coakley, S., Giordano-Santini, R., Linton, C., Lee, E.S., Nakagawa, A., Xue, D., and Hilliard, M.A. (2015). EFF-1-mediated regenerative axonal fusion requires components of the apoptotic pathway. Nature *517*, 219–222.

Nishi, T., and Forgac, M. (2002). The vacuolar (H+)-ATPases–nature's most versatile proton pumps. Nat. Rev. Mol. Cell Biol. *3*, 94–103.

Oren-Suissa, M., and Podbilewicz, B. (2010). Evolution of programmed cell fusion: common mechanisms and distinct functions. Dev. Dyn. *239*, 1515–1528.

Pellegrino, M.W., Farooqui, S., Fröhli, E., Rehrauer, H., Kaeser-Pebernard, S., Müller, F., Gasser, R.B., and Hajnal, A. (2011). LIN-39 and the EGFR/RAS/MAPK pathway regulate C. elegans vulval morphogenesis via the VAB-23 zinc finger protein. Development *138*, 4649–4660.

Pérez-Vargas, J., Krey, T., Valansi, C., Avinoam, O., Haouz, A., Jamin, M., Raveh-Barak, H., Podbilewicz, B., and Rey, F.A. (2014). Structural basis of eukaryotic cell-cell fusion. Cell *157*, 407–419.

Podbilewicz, B. (2014). Virus and cell fusion mechanisms. Annu. Rev. Cell Dev. Biol. *30*, 111–139.

Podbilewicz, B., and White, J.G. (1994). Cell fusions in the developing epithelial of C. elegans. Dev. Biol. *161*, 408–424.

Podbilewicz, B., Leikina, E., Sapir, A., Valansi, C., Suissa, M., Shemer, G., and Chernomordik, L.V. (2006). The C. elegans developmental fusogen EFF-1 mediates homotypic fusion in heterologous cells and in vivo. Dev. Cell *11*, 471–481.

Rasmussen, J.P., English, K., Tenlen, J.R., and Priess, J.R. (2008). Notch signaling and morphogenesis of single-cell tubes in the C. elegans digestive tract. Dev. Cell *14*, 559–569.

Rizvi, A.Z., Swain, J.R., Davies, P.S., Bailey, A.S., Decker, A.D., Willenbring, H., Grompe, M., Fleming, W.H., and Wong, M.H. (2006). Bone marrow-derived cells fuse with normal and transformed intestinal stem cells. Proc. Natl. Acad. Sci. USA *103*, 6321–6325.

Rual, J.F., Ceron, J., Koreth, J., Hao, T., Nicot, A.S., Hirozane-Kishikawa, T., Vandenhaute, J., Orkin, S.H., Hill, D.E., van den Heuvel, S., et al. (2004). Toward improving Caenorhabditis elegans phenome mapping with an ORFeome-based RNAi library. Genome Res. *14*, 2162–2168.

Sarov, M., Murray, J.I., Schanze, K., Pozniakovski, A., Niu, W., Angermann, K., Hasse, S., Rupprecht, M., Vinis, E., Tinney, M., et al. (2012). A genome-scale resource for in vivo tag-based protein function exploration in C. elegans. Cell *150*, 855–866.

Sato, M., and Sato, K. (2013). Dynamic regulation of autophagy and endocytosis for cell remodeling during early development. Traffic *14*, 479–486.

Sato, K., Norris, A., Sato, M., and Grant, B.D. (2014). C. elegans as a model for membrane traffic. WormBook, 1–47.

Satouh, Y., Inoue, N., Ikawa, M., and Okabe, M. (2012). Visualization of the moment of mouse sperm-egg fusion and dynamic localization of IZUMO1. J. Cell Sci. *125*, 4985–4990.

Schmid, S.L., Sorkin, A., and Zerial, M. (2014). Endocytosis: Past, present, and future. Cold Spring Harb. Perspect. Biol. *6*, a022509.

Shemer, G., and Podbilewicz, B. (2002). LIN-39/Hox triggers cell division and represses EFF-1/fusogen-dependent vulval cell fusion. Genes Dev. *16*, 3136–3141.

Shemer, G., Suissa, M., Kolotuev, I., Nguyen, K.C., Hall, D.H., and Podbilewicz, B. (2004). EFF-1 is sufficient to initiate and execute tissue-specific cell fusion in C. elegans. Curr. Biol. *14*, 1587–1591.

Shilagardi, K., Li, S., Luo, F., Marikar, F., Duan, R., Jin, P., Kim, J.H., Murnen, K., and Chen, E.H. (2013). Actin-propelled invasive membrane protrusions promote fusogenic protein engagement during cell-cell fusion. Science *340*, 359–363.

Shin, N.Y., Choi, H., Neff, L., Wu, Y., Saito, H., Ferguson, S.M., De Camilli, P., and Baron, R. (2014). Dynamin and endocytosis are required for the fusion of osteoclasts and myoblasts. J. Cell Biol. *207*, 73–89.

Shinn-Thomas, J.H., and Mohler, W.A. (2011). New insights into the mechanisms and roles of cell-cell fusion. Int. Rev. Cell Mol. Biol. *289*, 149–209.

Steinman, R.M., Brodie, S.E., and Cohn, Z.A. (1976). Membrane flow during pinocytosis. A stereologic analysis. J. Cell Biol. *68*, 665–687.

Traub, L.M. (2009). Tickets to ride: selecting cargo for clathrin-regulated internalization. Nat. Rev. Mol. Cell Biol. *10*, 583–596.

Verma, S.K., Leikina, E., Melikov, K., and Chernomordik, L.V. (2014). Late stages of the synchronized macrophage fusion in osteoclast formation depend on dynamin. Biochem. J. *464*, 293–300.

Walser, C.B., Battu, G., Hoier, E.F., and Hajnal, A. (2006). Distinct roles of the Pumilio and FBF translational repressors during C. elegans vulval development. Development *133*, 3461–3471.

Wassarman, P.M., and Litscher, E.S. (2008). Mammalian fertilization is dependent on multiple membrane fusion events. Methods Mol. Biol. *475*, 99–113.

Watanabe, S., Liu, Q., Davis, M.W., Hollopeter, G., Thomas, N., Jorgensen, N.B., and Jorgensen, E.M. (2013). Ultrafast endocytosis at Caenorhabditis elegans neuromuscular junctions. eLife *2*, e00723.

Weinstein, N., and Mendoza, L. (2013). A network model for the specification of vulval precursor cells and cell fusion control in Caenorhabditis elegans. Front. Genet. *4*, 112.

Yi, B., and Sommer, R.J. (2007). The pax-3 gene is involved in vulva formation in Pristionchus pacificus and is a target of the Hox gene lin-39. Development *134*, 3111–3119.

Zeev-Ben-Mordehai, T., Vasishtan, D., Siebert, C.A., and Grünewald, K. (2014). The full-length cell-cell fusogen EFF-1 is monomeric and upright on the membrane. Nat. Commun. *5*, 3912.

Zeigerer, A., Gilleron, J., Bogorad, R.L., Marsico, G., Nonaka, H., Seifert, S., Epstein-Barash, H., Kuchimanchi, S., Peng, C.G., Ruda, V.M., et al. (2012). Rab5 is necessary for the biogenesis of the endolysosomal system in vivo. Nature *485*, 465–470.

Zerial, M., and McBride, H. (2001). Rab proteins as membrane organizers. Nat. Rev. Mol. Cell Biol. *2*, 107–117.

Cell Reports, Volume *14*

Supplemental Information

RAB-5- and DYNAMIN-1-Mediated Endocytosis of EFF-1 Fusogen Controls Cell-Cell Fusion

Ksenia Smurova and Benjamin Podbilewicz

Supplemental information for

RAB-5- and DYNAMIN-1-Mediated Endocytosis of EFF-1 Fusogen Controls Cell-Cell Fusion

Ksenia Smurova[1] and Benjamin Podbilewicz[1]*

[1]Department of Biology, Technion-Israel Institute of Technology, Haifa 32000, Israel
*Author for correspondence (podbilew@technion.ac.il)

This file includes:
Supplemental Figures S1-S5
Supplemental Figure legends S1-S5
Supplemental Tables S1-S3
Movie legends S1-S6
Supplemental experimental procedures
Supplemental references

Supplemental Figures

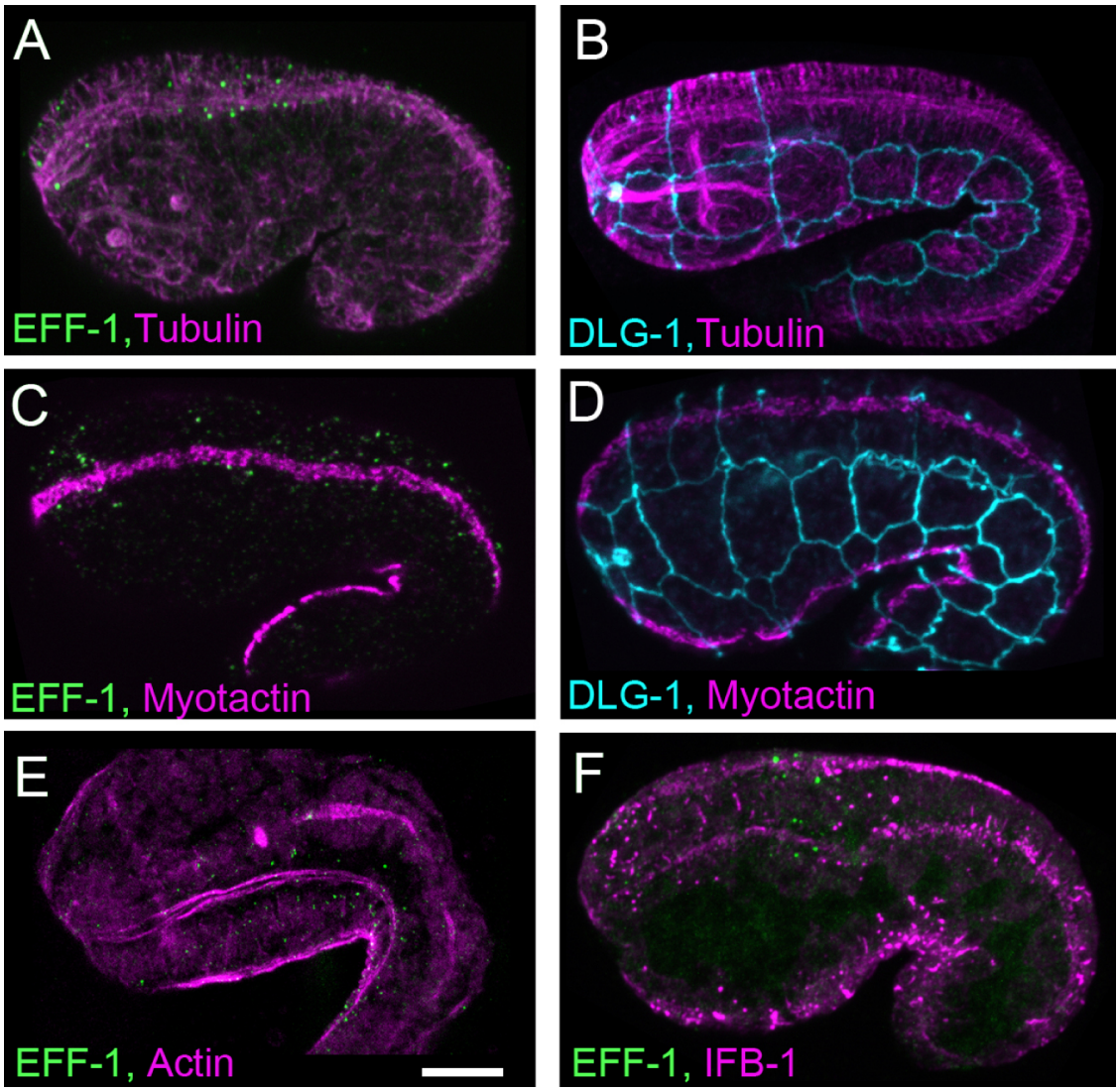

Figure S1. EFF-1 puncta arrangement along microtubule bundles, related to Figure 1
Organization of EFF-1 and cell junctions with respect to the cytoskeleton was analyzed by immunofluorescence. Scale bar, 10 μm.
(A) EFF-1 puncta along microtubule longitudinal bundles. Anti-EFF-1 antibody, green; anti-tubulin antibody, magenta.
(B) Bundles of microtubules localize parallel to the row of seam cells. Anti-tubulin antibody, magenta; anti-DLG-1 antibody, cyan.
(C) EFF-1 does not colocalize with fibrous organelles (hemidesmosome-like structures). Anti-EFF-1 antibody, green; anti-myotactin antibody, magenta.
(D) Fibrous organelles are aligned parallel to the row of seam cells. Anti-myotactin antibody, magenta; anti-DLG-1 antibody, cyan.
(E) EFF-1 does not colocalize with actin. Anti-EFF-1 antibody, green; Texas Red-phalloidin, magenta.
(F) Intermediate filaments do not show colocalization with EFF-1 puncta in embryos expressing IFB-1::GFP. Anti-EFF-1 antibody, green; anti-GFP antibody, magenta.

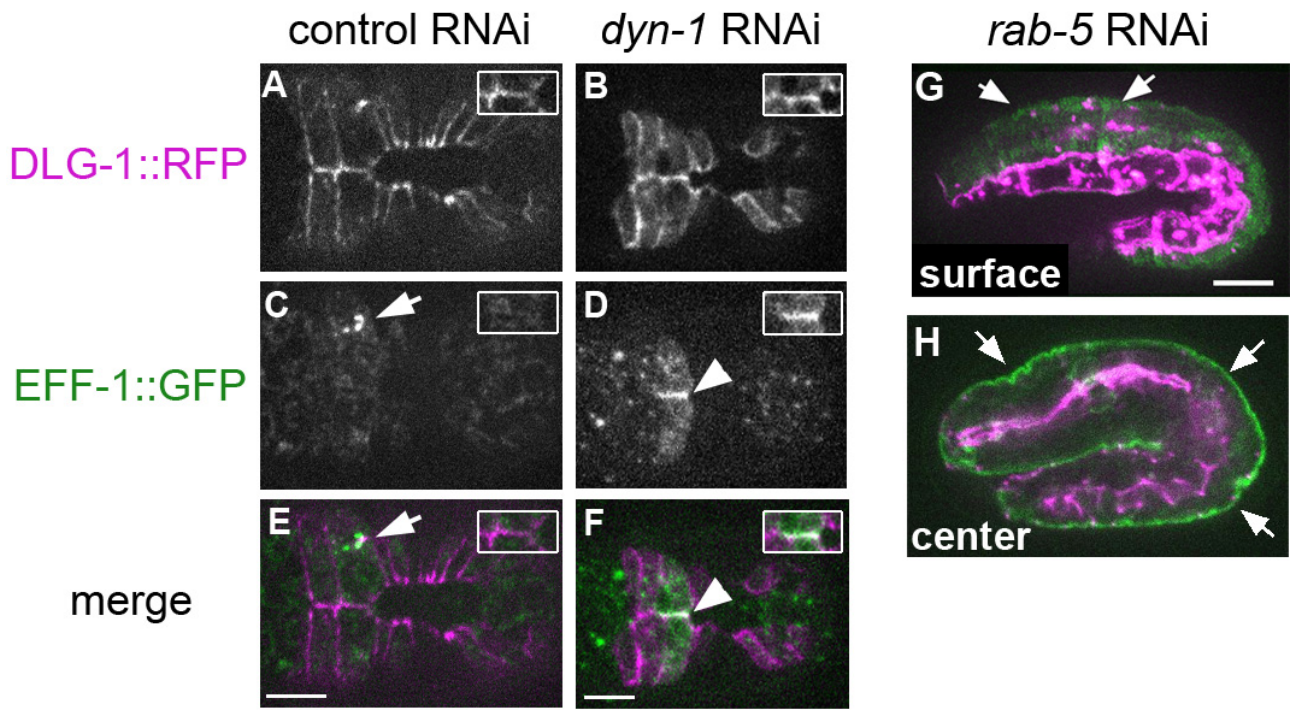

Figure S2. DYN-1 and RAB-5 knockdown induces EFF-1::GFP plasma membrane accumulation, related to Figure 2

(A-F) Ventral views of live embryos before the first fusion event under control RNAi and *dyn-1* RNAi treatment. Insets represent the areas of cell junctions between the cells in the process of fusion. EFF-1::GFP localize to cytoplasmic vesicles in control RNAi embryos (C, E, arrows). EFF-1::GFP shows plasma membrane mislocalization in *dyn-1* RNAi embryos (D, F arrowheads)

(G, H) EFF-1::GFP (green) and DLG-1::RFP (magenta) expression in *rab-5* RNAi treated embryos. Surface focus shows hyperfusion of hypodermal cells (G), center focus represents EFF-1 apical membrane localization (H, arrows; See also Movie S5). Scale bars, 10 μm.

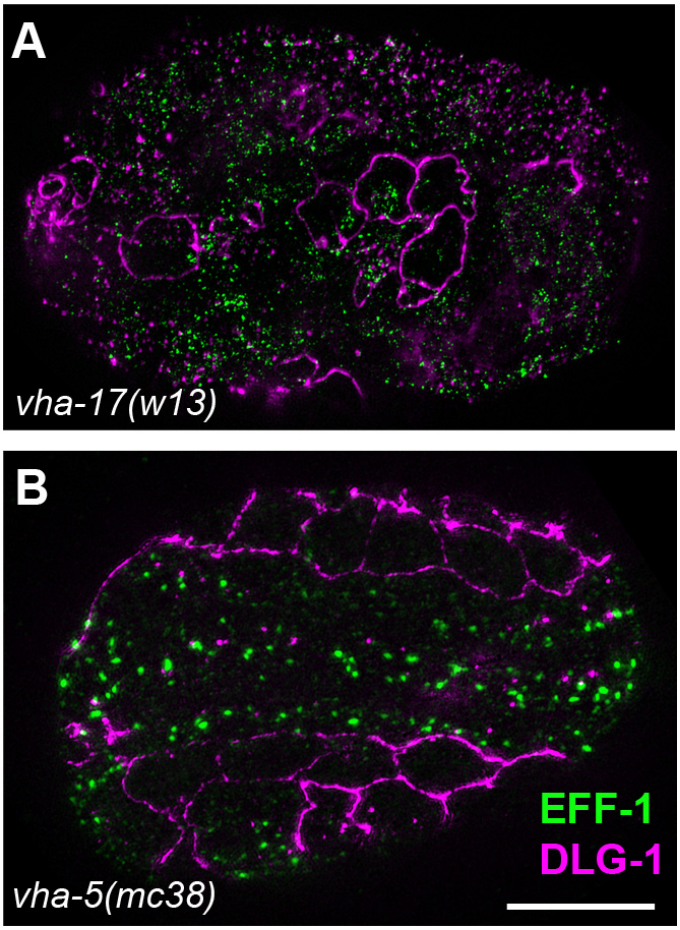

Figure S3. V-ATPase regulates cell fusion, related to Figure 3
Effect of mutations in two subunits of the vacuolar ATPase, VHA-17, and VHA-5, affect EFF-1 localization and fusion. Embryos were incubated at room temperature for 5-20 h and immunostained with anti-EFF-1 (green) and anti-DLG-1 antibody (magenta) followed SIM.
(A) Hyperfusion phenotype caused by *vha-17* mutation associates with smaller but denser EFF-1 puncta which did not colocalize with cell junctions.
(B) *vha-5* mutation induces hyperfusion but does not change EFF-1 localization.
Scale bar, 10 μm.

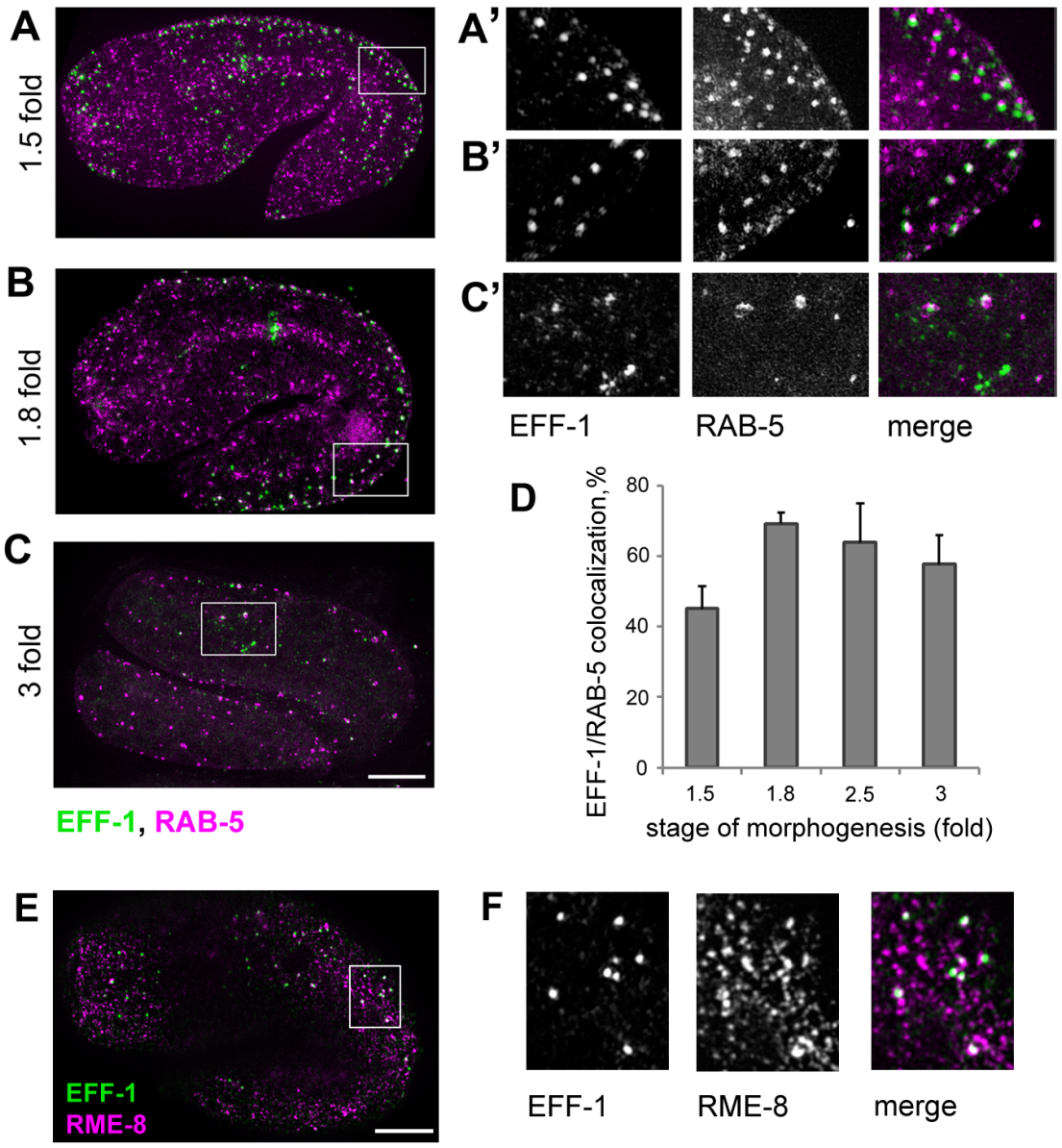

Figure S4. EFF-1/RAB-5 and EFF-1/RME-8 colocalization, related to Figure 4.
(A-C) EFF-1/RAB-5 colocalization changes in embryonic development. EFF-1 (green) and RAB-5 (magenta) colocalization at different stages of embryonic fusion was visualized by immunofluorescence with specific antibodies.
(A) 1.5 fold embryo
(B) 1.8 fold embryo
(C) 3 fold embryo
(A'-C') Enlargements of inset regions from (A-C) showing EFF-1, RAB-5 immunofluorescence, and merged images.
(D) Percentage of EFF-1 colocalization with RAB-5 during embryonic development (mean ± SEM). Number of puncta analyzed for each stage of morphogenesis was n>200.
(E) Colocalization of EFF-1 (green) with RME-8 (magenta, marker that is present in early, recycling, and late endosomes). EFF-1 and RME-8 patterns are visualized using immunofluorescence.
(F) Boxed region from (E) is enlarged and shown in separate channels: EFF-1, left; RME-8, middle; and merged, right.
Scale bars, 10 μm.

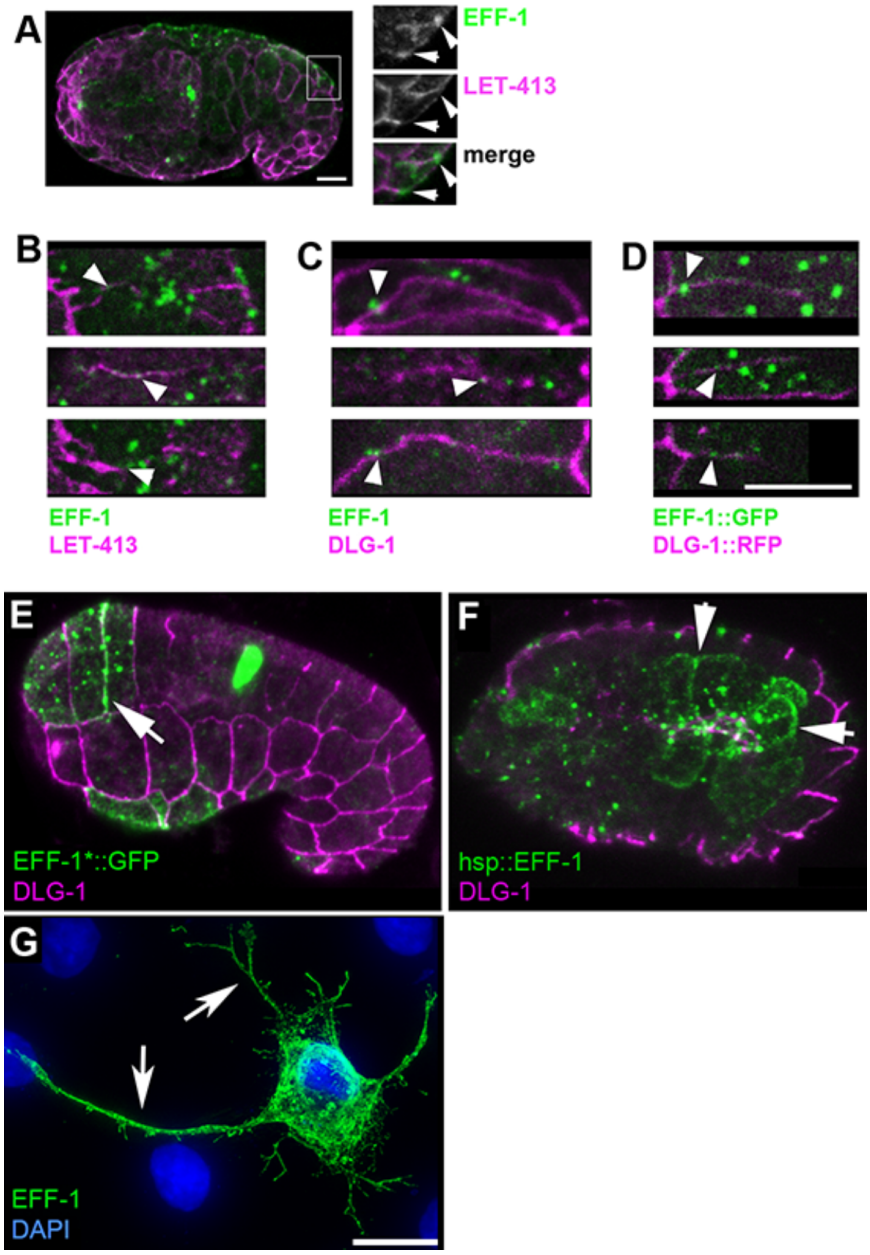

Figure S5. EFF-1 colocalization with membranes and apical junctions, related to Figure 6

(A) EFF-1 colocalization with basolateral membrane before fusion in LET-413::CFP expressing embryo is revealed by immunofluorescence with anti-EFF-1 (green) and anti-GFP antibody (LET-413, magenta).

(B-D) Individual confocal z-slices of cell junctions were taken from the dorsal side of embryos in the process of fusion. Enlarged areas of diverse junctions show partial EFF-1 colocalization with cell junctions (arrowheads).

(B) EFF-1 (green) and basolateral membrane marker LET-413::CFP (magenta) are visualized by immunofluorescence with anti-EFF-1 and anti-CFP antibody.

(C) Endogenous EFF-1 was immunolabled with anti-EFF-1 antibody, green; apical junctions were detected with anti-DLG-1 antibody, magenta.

(D) Live images of apical junctions (DLG-1::RFP, magenta) showing transient colocalization with EFF-1::GFP (green) prior to cell fusion.

(E) Nonfusogenic EFF-1::GFP* accumulation at the plasma membrane (arrow) in *C. elegans* embryo (*Del Campo et al., 2005). Immunofluorescence with anti-GFP antibody (green) and anti-DLG-1 (apical junction, magenta).

(F) Ectopic EFF-1 localization to the plasma membrane of intestinal cells (arrows) following heat shock in an embryo expressing *hsp::eff-1* transgene. (del Campo et al., 2005; Shemer et al., 2004). The projection of the z-slices of intestine is shown. Some intestinal cells have fused. Immunofluorescence with anti-EFF-1 antibody (green) and anti-DLG-1 (apical junction, magenta).

(G) Ectopic EFF-1 is detected in the plasma membrane of mammalian BHK cells transfected with *eff-1::*V5 construct (arrows). Immunofluorescence with anti-V5 antibody (green) and DAPI (nuclei, blue).

Scale bar represents 5 μm in (A-D) and 10 μm in (D-F).

Table S1

EFF-1 colocalization with cellular markers, related to Figure 4

Organelle (Ordered from highest to lowest)	**Strain**	**Protein**	**Mean (%) colocalization ±SEM**	**number of puncta**	**number of embryos**
Early endosome (EE)	RT122	RAB-5::GFP	58.2 ± 5.7	1766	21
Early endosome to MVB	DH1336	RME-8::GFP	30.3 ±7.3	436	6
Golgi	RT1315	MANS::GFP	19.2 ± 4.4	278	6
Lysosome	RT258	LMP-1::GFP	8.5 ± 3.3	272	6
Basolateral membrane	BP712	LET-413::CFP	8.3 ± 2.1	460	8
Apical junction	SU93	AJM-1::GFP	6.5 ± 2.3	803	11
Apical junction	N2	DLG-1 (Ab)	6.2 ± 1.7	534	9
Apical endosome	RT311	RAB-11::GFP	3.6 ± 1.5	273	5
EE from Golgi to PM	RT525	RAB-10::GFP	3 ± 0.9	408	5
Recycling endosome	RT348	RME-1::GFP	1.8 ± 0.04	378	5
Late endosome	RT476	RAB-7::GFP	1.9 ± 0.7	198	5
Autophagosome	BU071	LGG-1::GFP	1.7 ± 0.7	224	5
MVB	RT1356	ALX-1::GFP	1 ± 0.6	208	5
Vacuolar ATPase	ML846	VHA-5::GFP	0.9 ± 0.3	321	5
MVB	RT1341	HGRS-1::GFP	0 ± 0.04	98	5
Mitochondria	N2	HSP60-s (Ab)	No (visual observation)	-	12
Proteasome	N2	PAS-7 (Ab)	No (by visual observation)	-	15
ER	N2	CYP33E1-s (Ab)	No (by visual observation)	-	14
Endocytic invagination	N2	DYN-1 (Ab)	No (by visual observation)	-	10

Table S2
Hyperfusion and ectopic EFF-1 expression in trafficking mutants, related to Figure 3

Affected pathway	**Strain**	**Protein mutated (*allele*)**	**Hyperfusion**	**EFF-1 mislocalization to apical junctions**
Retrograde Golgi to ER	RB1535	ARF1.1(*ok1840*)	No	No
Early endocytosis	CX51	DYN-1(*ky51*)	**Yes**	**Yes**
Basolateral recycling	RT2	RAB-10(*q373*)	No	No
Basolateral recycling	VC1026	RAB-10(*ok1494*)	No	No
Recycling	DH1201	RME-1(*b1045*)	No	No
Early, recycling, late endocytosis	DH1206	RME-8(*b1023*)	No	No
Early endocytosis	VC2199	RAB-5(*ok2605*)	**Yes**	**Yes**
RAB-5 regulation	VC1282	RABX-5(*ok1763*)	No	No
Endocytic recycling	RT206	RAB-35(*b1013*)	No	No
Endocytic recycling	VC900	ALX-1(*gk412*)	No	No
To lysosome	GS2643	CUP-5(*ar465*)	No	No
Endosomal acidification, trafficking, apical secretion (V0-ATPase, subunit H)	JR2750	VHA-17/FUS-1(*w13*)	**Yes**	No
Endosomal acidification, trafficking, apical secretion (V0-ATPase, subunit A)	ML851	VHA-5(*mc38*)	**Yes**	No

Table S3
Fusion abnormalities and ectopic EFF-1 expression in embryos treated with RNAi, related to Figure 2

RNAi	Phenotype	Fusion defects in embryos (n)	Fusion defects in larvae (n)	EFF-1 mislocalization
rab-5	emb. lethal	yes (103)	-	yes
dyn-1	emb. lethal	yes (55)	-	yes
aps-1	no	no (45)	no (15)	no
syn-4	no	no (37)	no (10)	no
rab-6.1	no	no (35)	no (22)	no
rab-6.2	no	no (40)	no (15)	no
rme-6	no	no (48)	no (18)	no
rabx-5	no	no (42)	no (20)	no
bli-4 positive control	emb. lethal	no (20)	-	no
C06C3.5 negative control	no	no (20)	no (20)	no

Supplemental movie legends

Movie S1. EFF-1 dynamics during cell fusion, related to Figures 2 and 5
Time lapse recording of an *eff-1(hy21)II; mcIs46[dlg-1::RFP]; hyEx160[peff-1::eff-1::GFP]* transgenic embryo. EFF-1::GFP is shown in green, DLG-1::RFP is displayed in magenta. The z-series were recorded every 15 sec using spinning disk confocal microscopy, multiple intensity projection of a z-stack is shown at each time point. Lower panel represents enlarged area of the embryo (same embryo as in Figure 5). Arrows mark the start of apical junction disassembly. Time in minutes:seconds is shown at the top right corner.

Movie S2. EFF-1::GFP dynamics during late stages in syncytia formation in the dorsal hypodermis, related to Figure 2
Another embryo of an *eff-1(hy21)II; mcIs46[dlg-1::RFP]; hyEx160[peff-1::eff-1::GFP]* strain showing later stages of hypodermis fusion. Arrows indicate the beginning of apical junction disassembly. Microscopy and time interval as in **Movie S1**.

Movie S3. EFF-1 dynamics after RAB-5 depletion by RNAi, related to Figure 2E
Time lapse recording of an *eff-1(hy21)II; mcIs46[dlg-1::RFP]; hyEx160[peff-1::eff-1::GFP]* embryo after *rab-5*(RNAi) treatment. Green represents EFF-1::GFP, magenta shows DLG-1::RFP. The z-series were recorded every 30 seconds, lower panel represents enlarged area of the fusion (**Figure 2E**). Arrow marks the beginning of apical junction disassembly. Note the disappearance of the bright EFF-1::GFP puncta, the localization of EFF-1::GFP on the junctions and the increase of numerous small and less bright EFF-1::GFP vesicular staining.

Movie S4. *rab-5* depletion induces EFF-1 mislocalization to the apical plasma membrane and hyperfusion, related to Figures 2 and S2
Animated z-stack of an *eff-1(hy21)II; mcIs46[dlg-1::RFP]; hyEx160[peff-1::eff-1::GFP]* embryo treated with *rab-5* RNAi. All cells in the dorsal hypodermis are fused to each other (hyperfusion) in contrast to three unfused syncytia (*hyp5, 6,* and 7) in the *wt* embryos (**Figure 1A**). EFF-1 is expressed on plasma membrane of hypodermis syncytia. Maximum intensity projection of the dorsal side of this embryo is shown in Supplemental **Figure S2G, S2H**.

Movie S5. Apical membrane EFF-1 expression and hyperfusion induced by *dyn-1* RNAi, related to Figure 2F
Animated z-stack of live embryo expressing EFF-1::GFP and DLG-1::RFP after *dyn-1* RNAi treatment. This embryo shows EFF-1::GFP expression on the apical membrane, defects in embryogenesis, and hyperfusion.

Movie S6. *rab-5* RNAi depletion induce EFF-1::GFP accumulation to all surrounding apical membranes, related to Figure 6
Time lapse recording of an *eff-1(hy21)II; mcIs46[dlg-1::RFP]; hyEx160[peff-1::eff-1::GFP]* embryo after *rab-5*(RNAi) treatment. Green represents EFF-1::GFP, magenta shows DLG-1::RFP. The z-series were recorded every 30 seconds.

Supplemental experimental procedures

All nematode strains were maintained according to standard protocols (Brenner, 1974; Sulston and Hodgkin, 1988). In addition to the wild-type strain N2, the following mutations, transgenes and strains were used:

Markers of cell junctions and cytoskeleton

SU93	*jcIs1[ajm-1::gfp; unc-29(+); rol-6(su1006)]*	CGC; (Mohler et al., 1998)
ML1651	*mcIs46 [dlg-1::rfp; unc-119(+)]*	Michel Labouesse; (Diogon et al., 2007)
	let-413::cfp; rol-6	Olaf Bossinger; (Pilipiuk et al., 2009)
CZ3464	*ifb-1::gfp*	Limor Broday; (Woo et al., 2004)

EFF-1 alleles

BP75	*eff-1(hy21)II*	BP; (Mohler et al., 2002)
BP347	*eff-1(ok1021)II*	BP; (Podbilewicz et al., 2006)

Markers of intracellular organelles

DH1336	*bIs34[rme-8::GFP + rol-6(su1006)]*	CGC; (Zhang et al., 2001)
RT122	*pwIs20[GFP::rab-5 + unc-119(+)]*	CGC; (Sato et al., 2005)
RT311	*pwIs69[vha6p::GFP::rab-11 + unc-119(+)]*	CGC; (Chen et al., 2006)
RT476	pwIs170[*vha6p::GFP::rab-7 + Cb unc-119(+)]*	CGC; (Chen et al., 2006)
RT525	pwIs206[*vha6p::GFP::rab-10 + Cb unc-119(+)]*	CGC; (Chen et al., 2006)
RT1043	pwIs403[*Ppie-1::mCherry::rab-5 + unc-119(+)]*	CGC; (Sato et al., 2008)
RT1315	pwIs481[*Pvha-6::mans::GFP]*	CGC; (Chen et al., 2006)
RT258	pwIs50[*lmp-1::GFP + Cb-unc-119(+)]*	CGC; (Treusch et al., 2004)
DA2123	*Plgg-1;GFP::LGG-1;rol-6*	Hong Zhang; (Melendez et al., 2003)
RT1356	*pwIs524 (pvha-6::GFP::ALX-1)*	Barth Grant; (Shi et al., 2007)
RT4	*pwIs1 (palx-1::GFP::ALX-1)*	Barth Grant; (Shi et al., 2007)
RT1341	*pwIs518 (pvha-6::GFP::HGRS-1)*	Barth Grant; (Shi et al., 2007)
RT348	*pwIs87 (pvha-6::GFP::RME-1)*	Barth Grant; (Shi et al., 2007)
ML846	*vha-8(mc38)IV; mcEx337[vha-5(+)::GFP; rol-6(su1006)]*	CGC; (Liegeois et al., 2006)

Traffic mutants

CX51	*dyn-1(ky51) X*	CGC; (Clark et al., 1997)
VC900	*alx-1(gk412) III.*	CGC; (Shi et al., 2007)
RT2	*rab-10(q373) I*	CGC; (Chen et al., 2006)
DH1201	*rme-1(b1045) V.*	CGC; (Shi et al., 2007)
VC1026	*rab-10(ok1494) I.*	CGC; (Shi et al., 2012)
RB1535	*arf-1.1&F45E4.7(ok1840) IV*	CGC; (Sato et al., 2014)
ML732	*vha-5(mc38)/unc-24(e138) dpy-20(e1282) IV*	CGC; (Liegeois et al., 2006)
JR2750	*vha-17/fus-1(w13)*	Joel Rothman; (Kontani et al., 2005)
VC2199	*rab-5(ok2605) I/hT2[bli-4(e937) let-?(q782) qIs48](I;III)*	CGC; (Sato et al., 2014)
DH1206	*rme-8(b1023) I*	CGC; (Zhang et al., 2001)
VC1282	*rabx-5(ok1763) III*	CGC; (Sato et al., 2005)
RT206	*rab-35(b1013) III*	Barth Grant; unpublished

Strains constructed in this study:

BP953	*eff-1(hy21)II; mcIs46 [dlg-1::rfp; unc-119(+)]*	BP; this study
BP954	*eff-1(hy21)II; mcIs46; hyEx160[peff-1::eff-1::GFP]*	BP; this study
BP955	*rab-5(ok2605) I/hT2[bli-4(e937) let (q782) qIs48](I;III); mcIs46*	BP; this study
BP956	*rab-5(ok2605) I/hT2[bli-4(e937) let(q782) qIs48](I;III); eff-1(hy21)II; mcIs46[dlg-1::rfp; unc-119(+)]*	BP; this study

Immunofluorescence of *C. elegans* embryos

Eggs were collected by hypochlorite treatment of gravid adult worms and transferred to poly-lysine coated slides. Embryos were permeabilized by the freeze-crack method (Strome and Wood, 1983) and fixed in 100% methanol (5 min), 100% acetone (5 min) at -20°C. Slides were washed for 10 min with PBS, and blocked with blocking solution of 0.2% Ez-Block (Biological Industries, Israel) in PBST (PBS with 0.01% Tween). Slides were incubated for 1 h at room temperature with primary antibodies, washed three times for 10 min each with PBS at room temperature, and incubated at room temperature for 1 h with Alexa488, Alexa568, or Alexa647 conjugated α-mouse or α-rabbit secondary antibodies (Molecular Probes) in PBST. Slides were washed three times for 10 min each in PBST and mounted in Fluoromount-G (Southern Biotech). The following primary antibodies were used at the dilutions indicated: α-EFF-1 (ascites 20.10 from mouse; at 1:1000; Fridman et al., Submitted); MH27 (α-AJM-1, mouse, at 1: 500), α-GFP (rabbit; 1:500; MBL), α-tubulin (mouse, Sigma, 1:500). α-DLG-1 antibody (rabbit, at 1:400) is a kind gift from Olaf Bossinger. MH46 (α-myotactin, mouse, at 1: 400) is a kind gift from Limor Broday, Antibodies against C. elegans proteins CYP33E1-s, PAS-7, HSP60-s were obtained from Developmental Studies Hybridoma Bank (Hadwiger et al., 2010) and used in 1:10 dilution. Texas-red X phalloidin (Molecular probes) in final concentration of 0.2 µM was added with secondary antibody.

Cell culture, live imaging and immunofluorescence of BHK cells

Baby Hamster Kidney (BHK) cells and their growth conditions were according to standard protocols (Stoker and Macpherson, 1964). Cells were grown in Dulbecco's Modified Eagle's Medium (DMEM, Gibco) supplemented with 10% Fetal Bovine Serum, 2 mM L-Glutamine, 100 µg/ml Penicillin and 100 µg/ml streptomycin (Biological Industries, Kibbutz Beit Haemek, Israel) and sodium pyruvate (Gibco) in a humid atmosphere of 5% CO2 up to a maximal density of 10^6/ml. Cells were transfected with 2 µg/ml of *eff-1* pCAGGS DNA vector using Fugene 6 (Roche) at 1:4 ratio. After 24 hours of transfection the cells were fixed with 4% paraformaldehyde in PBS and

processed for immunofluorescence. Cells were incubated in 40 mM NH4Cl, washed in PBS, permeabilized in 0.1% tritonX-100 in PBS and blocked in 1% FBS in PBS. The coverslips were incubated 1 hour with anti-V5 1:500 (Invitrogen) mouse monoclonal antibodies at RT. The secondary antibodies were goat anti-mouse coupled to Alexa488 (Molecular Probes/Invitrogen), nuclei were visualized with DAPI (1 μg/ml) (Avinoam et al., 2011; Perez-Vargas et al., 2014).

Supplemental references

Avinoam, O., Fridman, K., Valansi, C., Abutbul, I., Zeev-Ben-Mordehai, T., Maurer, U.E., Sapir, A., Danino, D., Grunewald, K., White, J.M.*, et al.* (2011). Conserved eukaryotic fusogens can fuse viral envelopes to cells. Science *332*, 589-592.

Brenner, S. (1974). The genetics of Caenorhabditis elegans. Genetics *77*, 71-94.

Chen, C.C., Schweinsberg, P.J., Vashist, S., Mareiniss, D.P., Lambie, E.J., and Grant, B.D. (2006). RAB-10 is required for endocytic recycling in the Caenorhabditis elegans intestine. Mol Biol Cell *17*, 1286-1297.

Clark, S.G., Shurland, D.L., Meyerowitz, E.M., Bargmann, C.I., and van der Bliek, A.M. (1997). A dynamin GTPase mutation causes a rapid and reversible temperature-inducible locomotion defect in C. elegans. Proc Natl Acad Sci U S A *94*, 10438-10443.

del Campo, J.J., Opoku-Serebuoh, E., Isaacson, A.B., Scranton, V.L., Tucker, M., Han, M., and Mohler, W.A. (2005). Fusogenic activity of EFF-1 is regulated via dynamic localization in fusing somatic cells of C. elegans. Curr Biol *15*, 413-423.

Diogon, M., Wissler, F., Quintin, S., Nagamatsu, Y., Sookhareea, S., Landmann, F., Hutter, H., Vitale, N., and Labouesse, M. (2007). The RhoGAP RGA-2 and LET-502/ROCK achieve a balance of actomyosin-dependent forces in C. elegans epidermis to control morphogenesis. Development *134*, 2469-2479.

Gattegno, T. (2003). Isolation and characterization of cell-fusion mutants in C. elegans. In Biology (Technion).

Hadwiger, G., Dour, S., Arur, S., Fox, P., and Nonet, M.L. (2010). A monoclonal antibody toolkit for C. elegans. PLoS One *5*, e10161.

Kontani, K., Moskowitz, I.P., and Rothman, J.H. (2005). Repression of cell-cell fusion by components of the C. elegans vacuolar ATPase complex. Dev Cell *8*, 787-794.

Liegeois, S., Benedetto, A., Garnier, J.M., Schwab, Y., and Labouesse, M. (2006). The V0-ATPase mediates apical secretion of exosomes containing Hedgehog-related proteins in Caenorhabditis elegans. J Cell Biol *173*, 949-961.

Melendez, A., Talloczy, Z., Seaman, M., Eskelinen, E.L., Hall, D.H., and Levine, B. (2003). Autophagy genes are essential for dauer development and life-span extension in C. elegans. Science *301*, 1387-1391.

Mohler, W.A., Shemer, G., del Campo, J.J., Valansi, C., Opoku-Serebuoh, E., Scranton, V., Assaf, N., White, J.G., and Podbilewicz, B. (2002). The type I membrane protein EFF-1 is essential for developmental cell fusion. Dev Cell *2*, 355-362.

Mohler, W.A., Simske, J.S., Williams-Masson, E.M., Hardin, J.D., and White, J.G. (1998). Dynamics and ultrastructure of developmental cell fusions in the Caenorhabditis elegans hypodermis. Curr Biol *8*, 1087-1090.

Perez-Vargas, J., Krey, T., Valansi, C., Avinoam, O., Haouz, A., Jamin, M., Raveh-Barak, H., Podbilewicz, B., and Rey, F.A. (2014). Structural basis of eukaryotic cell-cell fusion. Cell *157*, 407-419.

Pilipiuk, J., Lefebvre, C., Wiesenfahrt, T., Legouis, R., and Bossinger, O. (2009). Increased IP3/Ca2+ signaling compensates depletion of LET-413/DLG-1 in C. elegans epithelial junction assembly. Dev Biol *327*, 34-47.

Podbilewicz, B., Leikina, E., Sapir, A., Valansi, C., Suissa, M., Shemer, G., and Chernomordik, L.V. (2006). The C. elegans developmental fusogen EFF-1 mediates homotypic fusion in heterologous cells and in vivo. Dev Cell *11*, 471-481.

Sato, K., Norris, A., Sato, M., and Grant, B.D. (2014). C. elegans as a model for membrane traffic. WormBook, 1-47.

Sato, M., Sato, K., Fonarev, P., Huang, C.J., Liou, W., and Grant, B.D. (2005). Caenorhabditis elegans RME-6 is a novel regulator of RAB-5 at the clathrin-coated pit. Nat Cell Biol *7*, 559-569.

Sato, M., Sato, K., Liou, W., Pant, S., Harada, A., and Grant, B.D. (2008). Regulation of endocytic recycling by C. elegans Rab35 and its regulator RME-4, a coated-pit protein. Embo j *27*, 1183-1196.

Shemer, G., Suissa, M., Kolotuev, I., Nguyen, K.C., Hall, D.H., and Podbilewicz, B. (2004). EFF-1 is sufficient to initiate and execute tissue-specific cell fusion in C. elegans. Curr Biol *14*, 1587-1591.

Shi, A., Liu, O., Koenig, S., Banerjee, R., Chen, C.C., Eimer, S., and Grant, B.D. (2012). RAB-10-GTPase-mediated regulation of endosomal phosphatidylinositol-4,5-bisphosphate. Proc Natl Acad Sci U S A *109*, E2306-2315.

Shi, A., Pant, S., Balklava, Z., Chen, C.C., Figueroa, V., and Grant, B.D. (2007). A novel requirement for C. elegans Alix/ALX-1 in RME-1-mediated membrane transport. Curr Biol *17*, 1913-1924.

Stoker, M., and Macpherson, I. (1964). SYRIAN HAMSTER FIBROBLAST CELL LINE BHK21 AND ITS DERIVATIVES. Nature *203*, 1355-1357.

Strome, S., and Wood, W.B. (1983). Generation of asymmetry and segregation of germ-line granules in early C. elegans embryos. Cell *35*, 15-25.

Sulston, J., and Hodgkin, J. (1988). Methods. In The Nematode Caenorhabditis elegans, W.B. Wood, ed. (Cold Spring Harbor: Cold Spring Harbor Laboratory), pp. 587-606.

Treusch, S., Knuth, S., Slaugenhaupt, S.A., Goldin, E., Grant, B.D., and Fares, H. (2004). Caenorhabditis elegans functional orthologue of human protein h-mucolipin-1 is required for lysosome biogenesis. Proc Natl Acad Sci U S A *101*, 4483-4488.

Woo, W.M., Goncharov, A., Jin, Y., and Chisholm, A.D. (2004). Intermediate filaments are required for C. elegans epidermal elongation. Dev Biol *267*, 216-229.

Zhang, Y., Grant, B., and Hirsh, D. (2001). RME-8, a conserved J-domain protein, is required for endocytosis in Caenorhabditis elegans. Mol Biol Cell *12*, 2011-2021.